

# Progress and Prospect of Sn-Based Metal-Organic Framework Derived Anode Materials for Metal-Ion Batteries

Weitao Zhang,<sup>[a]</sup> Yongyu Qi,<sup>[a]</sup> Jie Fang,<sup>[b]</sup> Wanxin Mai,<sup>[c]</sup> Xiaoming Lin,\*<sup>[c]</sup> Huachao Yang,\*<sup>[d]</sup> and Yongbo Wu<sup>[e]</sup>

In order to realize the growing demand for superior energy storage devices and electric vehicles, commercial anode candidates for next-generation rechargeable batteries need to meet the characteristics of low cost, high energy density, high capacity, and stable performance. The emerging tin-based anodes show great potential for high performance metal-ion battery anodes due to their high theoretical capacity, low cost, green harmless and high safety. Tin based anode materials include tin gold based materials, tin alloy materials, tin based oxides, tin based phosphide, tin based sulfides, multi-component composite materials, etc. However, the change in volume and structure of tin-based anode materials during the cycle has become the biggest obstacle to its development. Metal-organic frameworks (MOFs) provide a wide range of possibilities for

achieving high rate capacity and excellent cycle stability by finely regulating the structure and composition of tin-based materials at the molecular level. The latest progress of tin-based materials derived from MOFs as anode materials for metal-ion batteries (including lithium ion batteries, sodium ion batteries, potassium ion batteries, magnesium ion batteries) was reviewed in this paper. Firstly, the preparation method and morphology control of tin-based MOF are briefly introduced, and the structural characteristics, storage mechanism and modification of tin-based MOF derived materials are emphatically discussed. Finally, we summarized the existing modification measures and challenges of these anode materials, and put forward the prospect of the future.

## 1. Introduction

With the emergence of energy crisis and the development of environmental protection awareness, people need to seek various forms of energy other than traditional energy, and develop and utilize renewable energy on the basis of new technologies. Among them, the field of metal-ion batteries represented by lithium-ion batteries is a hot direction of research and development.<sup>[1–4]</sup> Metal-ion batteries have a high energy density, that is, the ability to store more energy in a relatively small volume or mass. This makes metal-ion batteries potentially advantageous in applications that require high energy density, such as electric vehicles and wearable devices.<sup>[5,6]</sup> In addition, the materials used in metal-ion batteries are relatively abundant and cheap, such as lithium, sodium and so on. Compared to the use of certain rare metals, the cost of metal-ion batteries may be lower, which is expected to reduce the overall cost of battery technology.<sup>[7,8]</sup> In addition, renewable energy storage, lightweight design and flexible design expand the application range of metal-ion batteries. Although metal-ion batteries have the above advantages, they also face some challenges, such as safety, cycle life, manufacturing costs and other issues.<sup>[9–11]</sup> In particular, anode materials for metal-ions still cannot meet practical needs. Researchers are constantly working to solve the problems of these anode materials to promote the commercialization and widespread application of metal-ion battery technology.

Sn-MOF is a metal-organic framework material composed of tin ions and organic ligands. Sn-MOF usually has a porous structure, which can provide more ion storage sites for metal-ions, helping to improve the capacity and charge and discharge

[a] W. Zhang, Y. Qi  
Luneng New Energy (Group) Co. LTD Qinghai Branch  
New Hualian International Center  
No. 61 Wusi West Road, Chengxi District  
Xining 810001, China

[b] J. Fang  
Power China Huadong Engineering Corporation Limited  
Hangzhou 311122, China

[c] W. Mai, Prof. X. Lin  
Key Laboratory of Theoretical Chemistry of Environment  
Ministry of Education  
School of Chemistry  
South China Normal University  
Guangzhou 510006, China  
E-mail: linxm@scnu.edu.cn

[d] Prof. H. Yang  
State Key Laboratory of Clean Energy Utilization  
College of Energy Engineering  
Zhejiang University  
Hangzhou 310027, China  
E-mail: huachao@zju.edu.cn

[e] Prof. Y. Wu  
Key Laboratory of Atomic and Subatomic Structure and Quantum Control  
(Ministry of Education)  
Guangdong Basic Research Center of Excellence for Structure and  
Fundamental Interactions of Matter  
School of Physics  
South China Normal University  
Guangzhou 510006, China  
Guangdong Provincial Key Laboratory of Quantum Engineering and  
Quantum Materials  
Guangdong-Hong Kong Joint Laboratory of Quantum Matter  
South China Normal University  
Guangzhou 510006, China

rate of the battery.<sup>[12,13]</sup> In addition, the MOF structure usually has a high surface area and aperture, which contributes to the rapid transmission and diffusion of lithium ions, thereby improving the charge and discharge performance of the battery.<sup>[14,15]</sup> In addition, the synthesis method of Sn-MOF is relatively flexible, and its structure and properties can be accurately controlled by regulating the selection of metal-ions and organic ligands as well as the adjustment of reaction conditions.<sup>[16,17]</sup> Finally, tin is a rich element, compared with rare metals (such as cobalt, nickel, etc.), the price of tin is lower, so the preparation cost of Sn-MOF may be lower, helping to reduce the overall cost of the battery.<sup>[18]</sup> In addition to inheriting the above advantages of the original MOF, Sn-MOF can be pyrolyzed to obtain different derivatives, including metals, oxides, sulfides, selenides, multi-component composites, etc. Tin-based materials have a high theoretical specific capacity, much higher than traditional carbon-based anode materials, thus improving the energy density of the battery (Figure 1a, 1b).<sup>[19–21]</sup> In addition, compared with other high-capacity alloy-type anodes, the higher voltage platform of tin-based anodes can inhibit the growth of lithium dendrites during battery discharge. This prevents the formation of lithium dendrites from causing battery capacity attenuation and internal resistance increase, as well as causing safety problems such as internal short circuit and thermal runaway of the battery. In recent years, Sn-MOF derivatives have been increasingly used in metal-ion battery anode materials. However, the synthesis, mechanism and electrochemical properties of Sn-MOF-derived tin-based materials in different metal-ion batteries still lack systematic induction and summary. Therefore, this paper reviews the panoramic design and latest progress of Sn-MOF derivatives as advanced energy storage materials (Figure 1c). Firstly, the synthesis scheme, morphology control and structure effect of Sn-MOF are introduced. Then, it focuses on the different storage processes (alloying and alloying-conversion reactions), microstructure, electrochemical properties and correlation of tin-based materials used in metal-ion batteries such as lithium ion batteries, sodium ion batteries, potassium ion batteries and so on. Finally, on this basis, the current challenges and the future direction of further development of Sn-MOF-derived tin-based electrodes are summarized and prospected.

## 2. Preparation Method and Morphology Control of Sn-MOF

Sn-MOFs consist of an Sn metal center connected to an organic ligand by coordination bonds. Tin metal is mainly derived from metal salts such as sulfate and chloride salts with valence states of +2 and +4. The organic ligands are mainly aromatic carboxylic acids such as 1, 4-phenyl dicarboxylic acid (1,4-BDC), 1, 2-phenyl dicarboxylic acid (1,2-BDC) and 1, 3, 5-phenyl tricarboxylic acid (BTC). A wet chemical process through simple "direct mixing" followed by stirring at room temperature for a period of time is the most convenient synthesis strategy for Sn-MOFs. Zhu *et al.* used  $\text{SnSO}_4$  dissolved in deionized water and mixed with terephthalic acid ( $\text{H}_2\text{BDC}$ ) solution to obtain okra pod-type Sn-MOF after mixing for several hours (Figure 2a).<sup>[30]</sup> During the synthesis process, an alkaline environment is usually required, so sodium hydroxide is added to adjust the acid alkalinity of the solution. In addition, the weak base  $\text{LiOH}$  is also another suitable choice. Sn-MOF grows on graphene oxide (GO) layers under the regulation of lithium hydroxide (Figure 2b).<sup>[31]</sup> In addition, Cheng *et al.* also used phthalic acid as an organic linker and synthesized Sn-MOF by adding polyvinyl pyrrolidone (PVP) modifier (Figure 2c).<sup>[32]</sup> Firstly, PVP can affect the morphology and size of MOF particles. The morphology of MOF, such as particle size, shape and surface structure, can be controlled by adjusting the concentration and synthesis conditions of PVP. Secondly, PVP, as a surfactant and template agent, can play a guiding role in the growth of MOF crystals. It can interact with metal ions or organic ligands to affect crystal growth kinetics and thermodynamics, thus controlling the morphology and crystal structure of MOF. Finally, in the synthesis process of MOF, PVP can be used as a dispersant to prevent the agglomeration and aggregation of MOF particles. In addition, hydrothermal or solvothermal method is a commonly used method for the preparation of metal-organic frames. Tin salt and organic ligand were dissolved in DI water (de-ionized water)/organic solvent according to a certain molar ratio, and the thermodynamic properties of solvent and the affinity between metal salt and ligand were used to promote the coordination reaction between them at high temperature to form Sn-MOF crystals. Fu *et al.* dissolved  $\text{H}_3\text{BTC}$  and  $\text{SnCl}_2 \cdot 2\text{H}_2\text{O}$  in methanol, transferred the mixed solution to the reactor for



**Xiaoming Lin** is a Professor at School of Chemistry, South China Normal University. After received his Ph.D. degree from Sun Yat-sen University, he remained a postdoctoral fellow at South China University of Technology and EVE Energy Co., Ltd. He also attended University of Science and Technology of China as well as Nanyang Technological University as a visiting scholar. His group aims to develop unique metal organic frameworks (MOFs) and their derivatives for electrochemical energy storage and conversion technology.



**Dr. Huachao Yang** is an Assistant Professor in College of Energy Engineering at Zhejiang University. He received his Ph.D. degree from Zhejiang University in 2018. During Ph.D. studies, he was a joint Ph.D. student at RWTH Aachen University. He was a Postdoctoral Associate at Zhejiang University from 2018 to 2021. His research focuses on the electrochemical energy storage devices (e.g., ion batteries and capacitors) and seawater desalination (CDI and solar-thermal desalination).

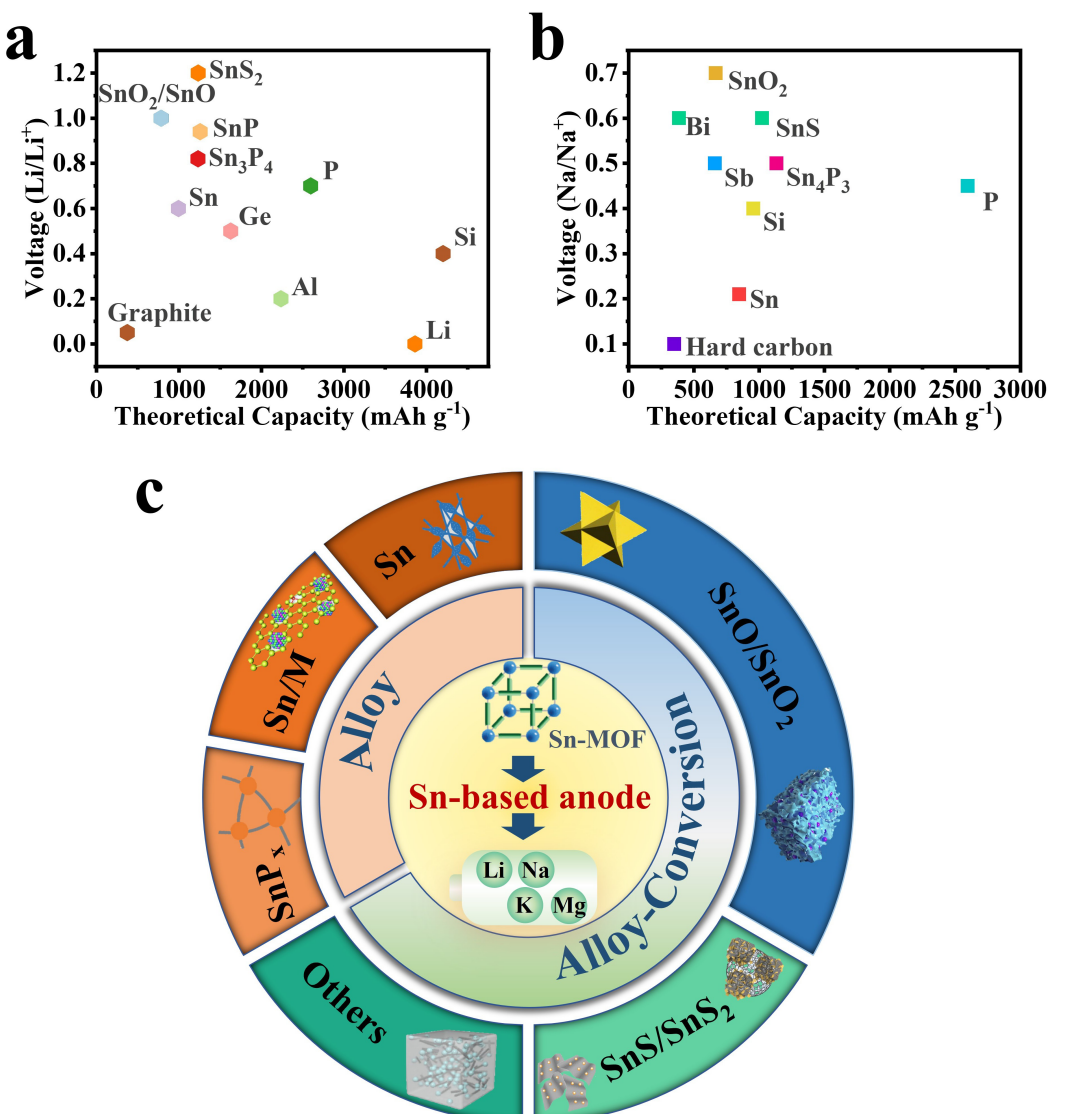


**Figure 1.** (a) Performance comparison of tin-based anodes with other anodes in LIBs. (b) Performance comparison of tin-based anodes with other anodes in SIBs. (c) Schematic illustration of the progress and prospect of Sn-MOFs derived tin-based anode materials.<sup>[22–29]</sup> Copyright 2018 Elsevier Ltd. Copyright 2021 Elsevier Ltd. Copyright 2023 Elsevier B.V. Copyright 2020 Elsevier B.V. Copyright 2019 Elsevier Ltd. Copyright 2023 Wiley-VCH GmbH. Copyright 2022 Wiley-VCH GmbH. Copyright 2022 The Authors. Published by Elsevier B.V.

solvothermal reaction after complete dissolving, and obtained spherical Sn-MOF precursor.<sup>[33]</sup> In addition, Sn-based MOF anode materials with high phase purity and large surface area can also be obtained by one-pot reflux method, which is also a simple and rapid synthesis strategy (Figure 2d).<sup>[16]</sup>

Microwave assisted solvent-thermal reaction is a method that uses microwave radiation heating to promote the MOF preparation process. Dai and collaborators obtained Ni-Sn-BTC MOF using a unique microwave assisted solvothermal reaction (Figure 3a).<sup>[34]</sup> Microspheres Ni-BTC MOFs were synthesized in a single-mode microwave reactor, and NiSn-BTC MOFs were synthesized by cation exchange reaction with Sn<sup>2+</sup> continuous magnetic stirring in the second reaction. Microwave assisted heating can uniformly heat the reaction system in a short time and improve the reaction rate. Compared with traditional heat sources, microwave can more effectively transfer energy to the

molecules in the reaction system, accelerate the chemical reaction, thus shortening the reaction time, being more energy efficient, and helping to reduce energy waste and environmental pollution.<sup>[35,36]</sup> In addition, Brainer used ultrasound to generate the mechanical effect of sound waves to promote the coordination of Na<sub>2</sub>BDC ligand salt and SnSO<sub>4</sub> to form Sn-BDC.<sup>[37]</sup> Ultrasonic assisted preparation of MOF is an efficient, controllable and environmentally friendly synthesis method, which has a wide application prospect in the preparation of MOF materials.

However, hot solvent synthesis relies on organic solvents, so it is difficult to avoid the environmental pollution and health problems that may be caused by the use and treatment of organic solvents, which is not in line with the principle of green synthesis. At the same time, the steps of volatilization and recovery of solvent increase the production cost and reduce the

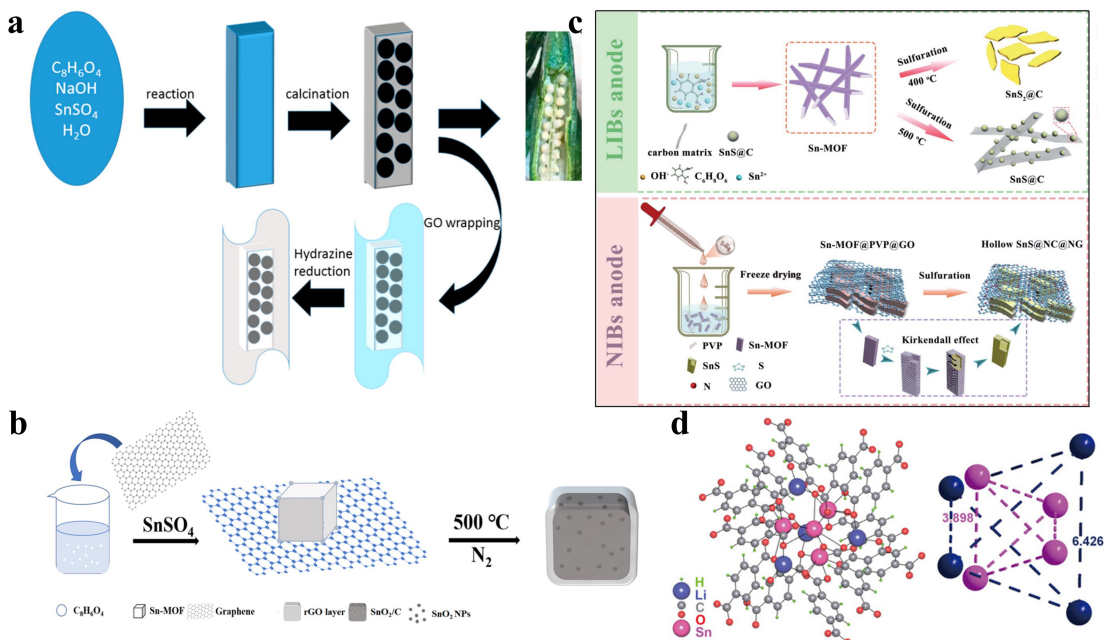


**Figure 2.** Schematic illustration of the fabrication process of (a)  $\text{SnO}_2@\text{N-RGO}$ .<sup>[30]</sup> Copyright 2017 American Chemical Society. (b)  $\text{SnO}_2/\text{C}/\text{rGO}$ .<sup>[31]</sup> Copyright 2021 IOP Publishing Ltd Printed in the UK. (c)  $\text{SnS}_2@\text{C}$ ,  $\text{SnS}@@\text{C}$  and  $\text{SnS}@@\text{NC}@@\text{NG}$ .<sup>[32]</sup> Copyright The Royal Society of Chemistry 2021. (d) Schematic illustration showing the structure of the Sn-MOF anode material.<sup>[16]</sup> Copyright 2018 Wiley-VCH Verlag GmbH & Co. KGaA, Weinheim.

efficiency of synthesis. Therefore, a simple two-step solvent-free heat treatment solid-phase synthesis method was developed to prepare Sn-MOF to avoid the above defects.<sup>[38]</sup> First,  $\text{CoSn}(\text{OH})_6$  and p-benzene dicarboxylic acid were mixed and then MOF was obtained by two-stage pyrolysis in air (Figure 3b).<sup>[38]</sup> The first heat treatment of  $\text{CoSn}(\text{OH})_6$  at  $300^\circ\text{C}$  first decomposed into  $\text{CoSnO}_3$ , and then underwent coordination reaction with  $\text{H}_2\text{BDC}$  organic ligand to form the MOF layer. The second stage of heat treatment at  $320^\circ\text{C}$  to remove impurities, while avoiding the temperature too high organic ligands do not melt and lead to solid-liquid phase aggregation and additional reactions. Through TEM test (Figure 3c, 3d), it can be observed that  $\text{SnO}_2/\text{Co}$  nanoparticles have an obvious complete carbon shell outside, and there are abundant cavities between the particles, and all elements are evenly distributed in the nanoparticles. Compared with liquid phase method, solvent-free method is more simple, does not need to deal with liquid solvent, improves the safety of operation, helps to reduce the environmental impact of the synthesis process, has good scalability, and is suitable for large-scale synthesis.

### 3. Metal-ion Batteries

#### 3.1. Lithium-ion batteries

Early on, due to the unmatched tunability, good morphology, and high porosity of the precursor, original Sn-MOFs were reported to be directly applied to anode materials for lithium-ion batteries.<sup>[16,39-43]</sup> However, the low conductivity and poor stability of MOFs themselves are unavoidable problems.<sup>[44,45]</sup>

After the thermal conversion of Sn-MOFs, the tin (Sn) based material can well preserve the special form of the precursor, while the target material after calcination improves the conductivity and stability, and is expected to be used as an anode material for advanced metal-ion batteries. Tin (Sn) based materials include metallic tin, tin alloy, tin oxide ( $\text{SnO}$ ,  $\text{SnO}_2$ ), tin sulfide ( $\text{SnS}$ ,  $\text{SnS}_2$ ), tin phosphide and its corresponding composite materials, multi-component composite materials, etc. Tin-based materials have potential advantages as anode materials for lithium-ion batteries. According to the storage mechanism, tin-based materials derived from Sn-MOFs are divided into alloy materials and alloy-conversion materials. The electrochemical properties of Sn-MOF derived tin-based materials in LIBs are shown in Table 1.

##### 3.1.1. Alloy Materials

As an anode material of lithium ion battery, pure tin has a high lithium ion storage capacity. Tin forms an alloy  $\text{Li}_{4.4}\text{Sn}$  with lithium during charging, which has a theoretical capacity of  $993 \text{ mAh g}^{-1}$ , and this alloying reaction is the main lithium storage mechanism.<sup>[46]</sup>  $\text{Sn} + x\text{Li}^+ + xe^- \leftrightarrow \text{Li}_x\text{Sn}$ . However, when pure tin is charged lithium ions become embedded in the tin's lattice spaces, which causes the tin to expand in volume. During the discharge process, lithium ions break away from the tin lattice and return to the electrolyte, and the volume of tin begins to shrink, resulting in the loosening of the structure between tin particles and the formation of microscopic cracks.<sup>[47,48]</sup> It results in particle breakage of the electrode material and instability of the electrode structure, which in turn

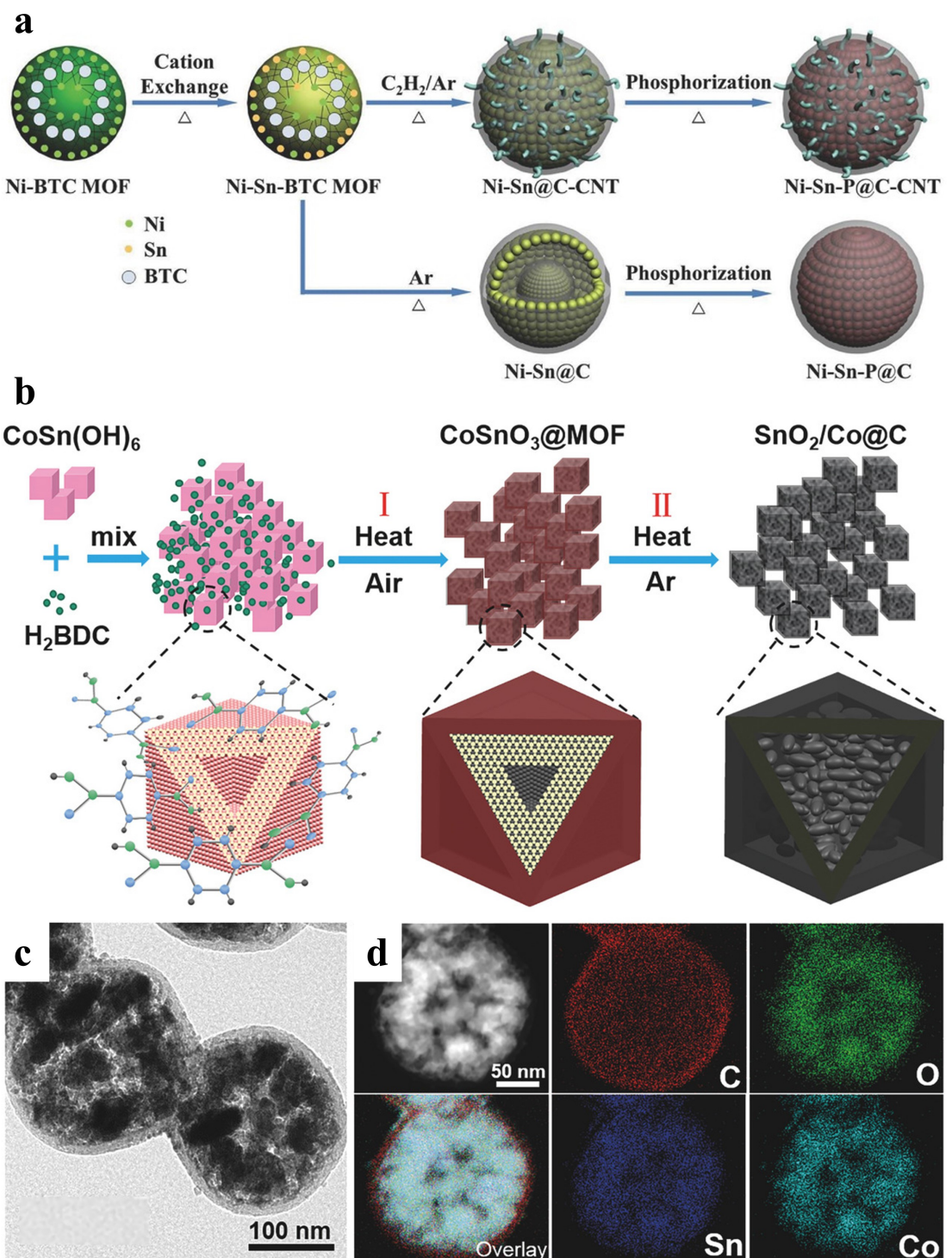


**Figure 3.** Schematic illustration of the fabrication process of (a) Ni-Sn-P@C-CNT.<sup>[34]</sup> Copyright 2017 Wiley-VCH Verlag GmbH & Co. KGaA, Weinheim. (b) SnO<sub>2</sub>/Co@C nanocubes. (c) TEM images together with (d) the corresponding elemental mappings.<sup>[38]</sup> Copyright 2017 Wiley -VCH Verlag GmbH & Co. KGaA, Weinheim.

affects the cycle life and performance of the battery. It is also a common problem that hinders the practical application of most metal/alloy-type electrode materials. To solve the problem of volume expansion of pure tin as the anode material of lithium-ion battery, the following optimization strategies can be adopted: (1) The introduction of carbon matrix into the tin-

based electrode material can effectively reduce the volume expansion of tin particles and prevent violent interaction between particles, which helps to maintain the stability of electrode structure and battery performance.<sup>[49–51]</sup> (2) Using nanomaterials technology, the volume expansion effect can be slowed down by controlling the particle size and shape of tin.

**Table 1.** Electrochemical properties of Sn-MOF derived tin-based materials in LIBs.

| Materials                                                                                                            | The ligand of Sn-MOF                       | Initial DC/CC<br>(mAh g <sup>-1</sup> ) | ICE<br>(%) | CD(mA g <sup>-1</sup> )/CR/<br>RC (mAh g <sup>-1</sup> ) | Storage<br>mechanism | Reference |
|----------------------------------------------------------------------------------------------------------------------|--------------------------------------------|-----------------------------------------|------------|----------------------------------------------------------|----------------------|-----------|
| SnO/C                                                                                                                | terephthalic acid(1,4-BDC)                 | 1368/1040                               | 76         | 100/100/950                                              | alloy-conversion     | 22        |
| SnO <sub>2</sub> QDs@C<br>(SnO <sub>2</sub> quantum dots embedded in carbon martix)                                  | 1,3,5-trimeric acid(BTC)                   | 1663.0/<br>1363.66                      | 82         | 200/200/1337                                             | alloy-conversion     | 24        |
| Sn/SnO@C                                                                                                             | o-phthalic acid(1,2-BDC)                   | 2089 /1015                              | 49         | 1000/200/ 835.9                                          | alloy-conversion     | 25        |
| SnO@C                                                                                                                |                                            | 2095.3/835.6                            | 39.9       | 1000/200/570.3                                           | alloy-conversion     |           |
| Sn@C                                                                                                                 |                                            | 1984.5/1146.3                           | 57.8       | 1000/200/437.2                                           | alloy                |           |
| FeSn <sub>2</sub> /FeSn/Fe                                                                                           | K3[Fe(CN)6]                                | 1930/1243                               | 64.4       | 200/200/1274                                             | alloy                | 26        |
| SnS <sub>2</sub> /C/CNT<br>SnS <sub>2</sub> /carbon/(carbon nanotubes)                                               | terephthalic acid(1,4-BDC)                 | 1689.7/1017.2                           | 60.2       | 200/100/954.2                                            | alloy-conversion     | 27        |
| SnP/CNTs<br>(tin phosphide /carbon nanotubes)                                                                        | terephthalic acid(1,4-BDC)                 | 1899/813                                | 42.8       | 1000/100/430                                             | alloy                | 29        |
| SnO <sub>2</sub> @N-RGO<br>(nitrogen-doped graphene wrapped okra-like SnO <sub>2</sub> )                             | o-phthalic acid(1,2-BDC)                   | 2217/1363                               | 61.5       | 200/180/1041                                             | alloy-conversion     | 30        |
| SnO <sub>2</sub> /C/rGO<br>(double carbon conductive network-encapsulated SnO <sub>2</sub> )                         | terephthalic acid(1,4-BDC)                 | –                                       | –          | 500/150/720.2                                            | alloy-conversion     | 31        |
| SnS <sub>2</sub> @C                                                                                                  | o-phthalic acid(1,2-BDC)                   | 1788.4/1238.2                           | 69.2       | 100/100/1200                                             | alloy-conversion     | 32        |
| Sn-MOF-250                                                                                                           | 1,3,5-trimeric acid(BTC)                   | –                                       | –          | 100/110/846.6                                            | alloy-conversion     | 33        |
| Ni-Sn-P@C-CNT<br>(carbon coated NiP <sub>2</sub> /Ni <sub>3</sub> Sn <sub>4</sub> with deep-rooted carbon nanotubes) | 1,3,5-trimeric acid(BTC)                   | 1402/933                                | 66.5       | 100/200/415                                              | alloy                | 34        |
| SnO <sub>2</sub> /Co                                                                                                 | terephthalic acid(1,4-BDC)                 | ≈1300/≈857                              | 66         | 200/100/800                                              | alloy-conversion     | 38        |
| Sn@C@CNF                                                                                                             | terephthalic acid(1,4-BDC)                 | 1076.3/891.2                            | 83.2       | 200/180/610.8                                            | alloy                | 54        |
| Sn@NPC<br>(ultrasmall Sn nanodots in the nitrogen-doped porous carbon matrix)                                        | terephthalic acid(1,4-BDC)                 | 1192/706                                | 59.2       | 200/500/575                                              | alloy                | 55        |
| Sn-Co@C                                                                                                              | 2-methylimidazole (2-MIM)                  | 822/1260                                | 65         | 0.2 C/200/ 763                                           | alloy                | 61        |
| SnO <sub>2</sub> /C/RGO<br>( SnO <sub>2</sub> /C/reduced graphene oxide)                                             | 3,4,5-trihydroxybenzoic acid               | 976.6/1551.9                            | 62.9       | 1000/700/823.6                                           | alloy-conversion     | 66        |
| MOF-SnO <sub>2</sub> NP/SSSC<br>(MOF-SnO <sub>2</sub> nanoparticles/sunflower seed shell porous carbon)              | terephthalic acid(1,4-BDC)                 | 2491.1/1424                             | 57.17      | 2 C/1000/512.9                                           | alloy-conversion     | 67        |
| Sn@C-800<br>(Sn@C at 800 °C)                                                                                         | 2,2'-Thiodiacetic acid                     | 1951/1558                               | 65         | 1000/1000/637                                            | alloy                | 72        |
| SnO <sub>2</sub> /SnO@C                                                                                              | 1,2,4,5-benzene-tetracarboxylic acid (PTA) | 1567.1/987.3                            | 63.0       | 200/100/611.9                                            | alloy-conversion     | 76        |
| SnS <sub>2</sub> /C                                                                                                  | terephthalic acid(1,4-BDC)                 | 1879.6/1121.6                           | 59.6       | 100/100/847.9                                            | alloy-conversion     | 80        |
| Zn <sub>2</sub> SnO <sub>4</sub> @C/Sn                                                                               | terephthalic acid(1,4-BDC)                 | –                                       | –          | 100/100/1140                                             | alloy-conversion     | 83        |

DC/CC: Discharge capacity/Charging capacity, ICE: Initial coulomb efficiency, CD: Current density, CR: Cycle number, RC: Reversible capacity.

Nanostructured materials have a larger surface area and a shorter ion diffusion path, thus improving electrode stability.<sup>[52]</sup>

(3) Optimizing the structural design of the electrode, such as the design of the layer structure, nanowire structure or porous structure, can improve the diffusion rate of lithium ions and the

stability of the electrode, and slow down the volume expansion effect.<sup>[53]</sup>

According to the above, zhu et al used the electrospinning strategy to derive Sn nanoparticles of cross-linked one-dimensional carbon nanofibers (Sn@C@CNF) from Sn-MOF, as shown

in Figure 4a.<sup>[54]</sup> The derived products retain the porous MOF structure, and form micropores on the surface and hollow carbon nanofibers inside, which limits the volume change of the composite and maintains the mechanical integrity of the composite. At the same time, the nanoparticles with good dispersion can improve the capacity retention and life of tin-based electrode materials. After 180 cycles at a current of 200 mA g<sup>-1</sup>, Sn@C@CNF has a stable specific discharge capacity of 610.8 mAh g<sup>-1</sup> (Figure 4b). It is worth noting that the one-dimensional structure electrode can adapt to large deformation, provide good compliance and strong adhesion, and promote the further development of flexible electronic devices. In addition, Dai et al reported that a composite material loaded with uniformly dispersed Sn nanodots in N-doped mesoporous

carbon matrix (Sn@NPC) was derived from a metal-organic framework as a high-performance electrode material for lithium ion storage (Figure 4c).<sup>[55]</sup> Among them, N doping is due to the addition of dicyandiamide during the pyrolysis process to transform into layered graphitic carbon nitride. Ultra-small size Sn nanodots avoid (2–3 nm) crushing and aggregation during alloying/dealloying process. Nitrogen-doped carbon not only improves the electrical conductivity of the material and enhances the electron transport capability, thus increasing the conductivity of the electrode. It can also increase the lithium ion adsorption sites on the surface of the electrode material, reduce the side reaction between the electrode material and the electrolyte, and promote the diffusion and migration of lithium ions in the electrode material.

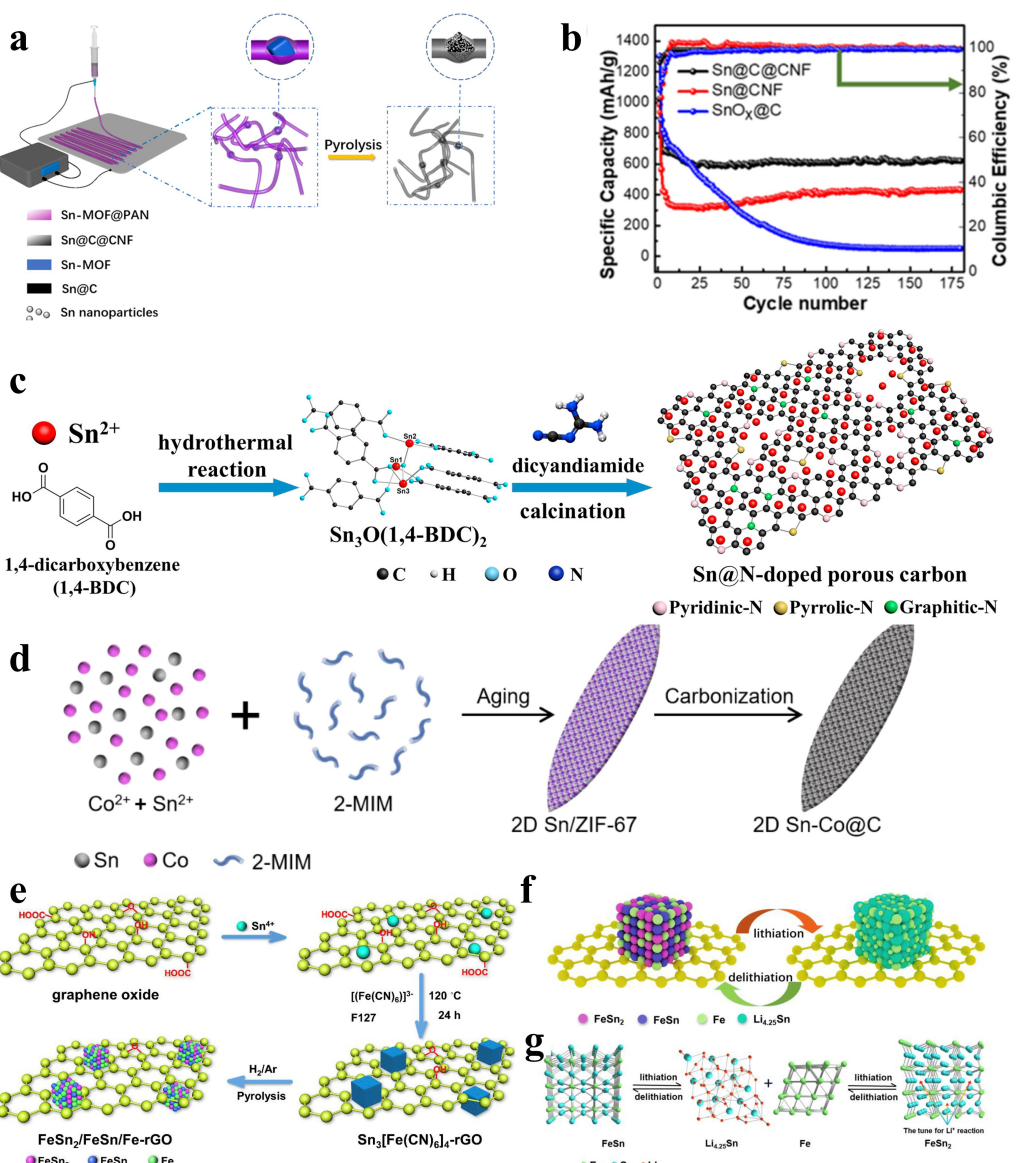


**Figure 4.** (a) Schematic illustration of the fabrication process of the flexible Sn@C@CNF film. (b) Specific capabilities at various current densities.<sup>[54]</sup> Copyright 2021 IOP Publishing Ltd. (c) Schematic illustration of the fabrication process of Sn nanodots embedded in N-doped mesoporous carbon.<sup>[55]</sup> Copyright 2016 Published by Elsevier Ltd. (d) Schematic illustration of the fabrication process of Co@C and Sn-Co@C.<sup>[61]</sup> Copyright 2022 Elsevier Ltd. (e) Schematic illustration of the fabrication process of the FeSn<sub>2</sub>/FeSn/Fe-rGO. (f) Schematic diagram of the lithiation-delithiation processes (g) Schematic illustration of the crystallographic changes during charge/discharge processes.<sup>[26]</sup> Copyright 2019 Elsevier Ltd.

In order to overcome the volume stress problem, the introduction of inactive or less active transition metal Sn–M phase (M=Fe, Mn, Cu, Ni, Co, etc.) is also an effective optimization strategy.<sup>[56–60]</sup> Forming an alloy of tin with other metals can improve its structural stability, reduce the volume expansion stress and harmful comminution, and thus improve the cyclic stability and structural strength of the electrode material. Sn–M alloying can adjust the electronic structure and ion transport performance of the material, thereby improving the electrochemical performance of the battery, such as increasing the conductivity and ion diffusion coefficient of the electrode, increasing the discharge capacity and cycle life of the battery. Compared with traditional preparation methods, MOF derivations can ensure uniform dispersion of different metal components, avoid nanoparticle aggregation and strengthen the connection between the active substance and the supporting substrate.

Using bimetallic MOFs, Gao and collaborators developed a tin-cobalt alloy embedded in a two-dimensional leaf nitrogen-doped carbon framework (Figure 4d).<sup>[61]</sup> This feasible method integrates uniformly distributed Sn–Co alloy particles, two-dimensional foliated carbon framework and n doping into a whole, and each component has a synergistic effect. Predictably, lithium-ion batteries based on Sn–Co@C composite electrodes demonstrate outstanding lithium storage performance and significant reversible capacity. A considerable reversible capacity of 604 mAh g<sup>-1</sup> is maintained even after 700 cycles, which shows good long-term stability. Similarly, Xu and team first synthesized the Prussian blue precursor Sn<sub>3</sub>[Fe(CN)<sub>6</sub>]<sub>4</sub>/rGO on reduced graphene oxide (rGO), and then derived the nanoalloy composite (FeSn<sub>2</sub>/FeSn/ Fe-RGO), as shown in Figure 4e.<sup>[26]</sup> In order to improve reduction efficiency, the precursor is the end product of thermal decomposition in an Ar/H<sub>2</sub> atmosphere. As anode material in LIBs, FeSn<sub>2</sub>/FeSn/Fe-rGO composite material has high specific capacity, good initial coulomb efficiency, superior rate capability. This is because rGO acts as a two-dimensional elastic matrix to buffer the bulk expansion and structural combusting of the electrode during the cycle (Figure 4f, 4g). Like the former, the introduction of the inert metal Fe and its formation of FeSn<sub>2</sub> and FeSn can not only provide good electronic conductivity and lithium ion diffusion, but also adapt to the volume expansion of the alloy reaction.

The electrochemistry of tin phosphide (SnP<sub>x</sub>) as an anode material in lithium-ion batteries involves lithium ion dealloying and dealloying processes. In charging, lithium ions form Li<sub>x</sub>SnP compounds by embedding into the lattice of tin phosphide. In contrast to the charging process, lithium ions detach from the Li<sub>x</sub>SnP compound during discharge, causing the volume of the anode material to shrink. As a result, SnP as an anode material has a high theoretical specific capacity (1255 mAh g<sup>-1</sup>) and a low potential, which makes it a potential material for high energy density batteries.<sup>[29]</sup> SnP also have problems with volume expansion and contraction, which may lead to peeling of electrode particles and attenuation of battery performance.<sup>[62,63]</sup> Zhao *et al.* reported the preparation of tin phosphide/carbon nanotubes (SnP/CNTs) using Sn-MOF as a template by adjusting the phosphorus/carbon ratio.<sup>[29]</sup> Carbon

nanotubes are used as a support and conductive network for small tin particles to increase electron transmission speed and help maintain structural stability during lithiation/demineralization. The SnP/CNTs composites were prepared with high reversible capacity (1899 mAh g<sup>-1</sup> capacity at 100 mA g<sup>-1</sup>) and good rate capability (610 mAh g<sup>-1</sup> capacity at 2000 mA g<sup>-1</sup>). In addition, SnP/CNTs were used as anode materials to assemble full batteries, which showed a high working capacity of about 292 mAh g<sup>-1</sup> and a capacity retention rate of 80.5%.

### 3.1.2. Alloy-conversion Materials

Alloy-converted materials are special as LIBs anode materials, involving two storage mechanisms, including conversion reactions and alloying reactions. In the process of charging and discharging, the mixed material will undergo a conversion reaction, that is, lithium ions are embedded in the lattice during charging to form Li compounds. During discharge, the lithium ions are removed from the Li compound and returned to the electrolyte. In addition to conversion reactions, hybrid materials can also form alloys with lithium. When charging, it can form an alloy with lithium, and at the end of charging, the lithium can be detached from the alloy. Tin oxide (SnO<sub>2</sub>) is a familiar alloy-conversion material that is often used as an anode material for lithium-ion batteries. SnO<sub>2</sub> has a high theoretical capacity (~782 mAh g<sup>-1</sup>), which makes SnO<sub>2</sub> theoretically capable of providing a higher battery energy density.<sup>[50]</sup> In lithium-ion batteries, SnO<sub>2</sub> will undergo a conversion reaction with lithium ions during charging and discharging. During the charging process, SnO<sub>2</sub> chemically reacts with lithium ions to form the metal tin (Sn) and lithium oxide. The metal tin is reversibly alloyed with Li. During the discharge process, the metal tin reacts with lithium ions to regenerate SnO<sub>2</sub>. Specifically, SnO<sub>2</sub> + 4Li<sup>+</sup> + 4e<sup>-</sup> → Sn + 2Li<sub>2</sub>O·Sn + xLi<sup>+</sup> + xe<sup>-</sup> ↔ Li<sub>x</sub>Sn. However, a major challenge for materials is that due to volume changes during insertion and removal, the electrode material may be structurally damaged, thus affecting the cycle performance of the battery.<sup>[64,65]</sup>

In order to improve the performance of SnO<sub>2</sub> as an anode material for lithium-ion batteries, a series of strategies such as graphitized carbon, carbon nanotubes and graphene oxide are usually employed to coat/wrap/compound SnO<sub>2</sub> with carbonaceous materials. Fu *et al.* prepared spherical Sn-MOF precursor by hydrothermal method, and investigated the electrochemical performance of SnO<sub>2</sub> at different annealing temperatures of 200, 250 and 300 °C.<sup>[33]</sup> The results showed that the tin dioxide derived at 250 °C had excellent cycling performance, and reached a reversible capacity of 846.6 mAh g<sup>-1</sup> after 110 cycles at 0.1 A g<sup>-1</sup>. This depends on the highly porous structure of Sn-MOF-250 and its ability to maintain the morphology of the precursor to the greatest extent. This emphasizes the importance of selecting the pyrolysis temperature of MOF derivatives and provides an alternative way to control the structure and properties of MOF. In order to enhance the conductivity and structural stability of the SnO<sub>2</sub> composite electrode, additional different C sources are added during the synthesis process. For

example, Zhu and group grew Sn-MOF on a two-dimensional (2D) graphene oxide (GO) material, which was converted into a porous carbon shell  $\text{SnO}_2$ .<sup>[31]</sup> Due to the extremely high electrical conductivity of reduced graphene (about  $20,000 \text{ cm}^2 \text{ V}^{-1} \text{ s}^{-1}$ ),  $\text{SnO}_2$  has significant electrochemical capabilities as an anode component of lithium-ion batteries. In addition, Yu *et al.* added gallic acid (3,4,5-trihydroxybenzoic acid,  $\text{C}_7\text{H}_6\text{O}_5$ , GA) on the basis of graphene oxide to compound Sn-MOF (Figure 5a).<sup>[66]</sup> Gallic acid (GA) molecules come from natural plants, are abundant, green, and have coordination effects with metal atoms or ions, while also optimizing the surface properties of RGO tablets (Figure 5c). As shown in Figure 5b, the reversible capacity of  $\text{SnO}_2/\text{C}/\text{RGO}$  samples is

about  $412.2 \text{ mAh g}^{-1}$  when the current density is  $2 \text{ A g}^{-1}$ , respectively, showing good rate performance. Similarly, Liang and collaborators used sunflower seed shell porous carbon (SSSC) as a biomass carbon source to improve the expansion of the anode and improve the conductivity of tin oxide.<sup>[67]</sup> Biomass materials are usually derived from renewable resources, such as plants, wood, waste, etc. Compared with traditional mineral anode materials, the use of biomass materials helps to reduce the dependence on limited natural resources, in line with the concept of sustainable development.<sup>[68]</sup> Interestingly, Hong *et al.* adopted a simple and rapid microwave-assisted method to prepare the tin dioxide/carbon anode, abandoning the traditional programmed heating method and hydrothermal

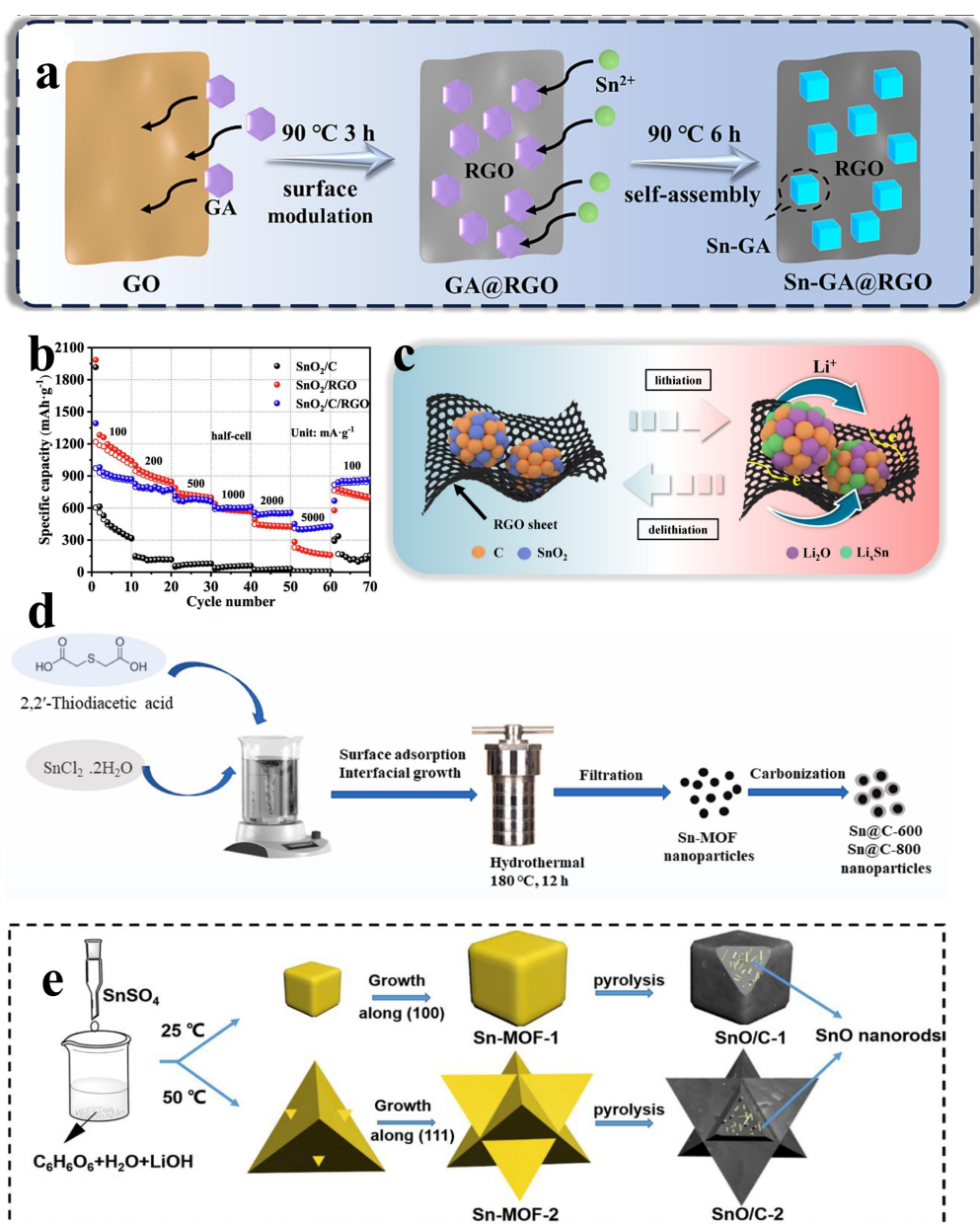


**Figure 5.** (a) Schematic illustration for the formation mechanism of the Sn-GA@RGO sample. (b) rate capabilities. (c) Illustration of the lithiation/delithiation process.<sup>[66]</sup> Copyright 2023 Elsevier Inc. (d) Schematic illustration of the fabrication process of Sn@C-600, and Sn@C-800 nanoparticles.<sup>[72]</sup> Copyright 2022 Elsevier Masson SAS. (e) Schematic illustration of the fabrication process of Sn-MOFs and SnO/C polyhedrons [22]. Copyright 2018 Elsevier Ltd.

method which are time-consuming, high energy consumption and unstable yield.<sup>[24]</sup> Sn-MOF is synthesized at room temperature and decomposed into SnO<sub>2</sub> QDs@C within tow seconds by microwave. The fully reversible conversion reaction was realized through the nanoscale engineering of dispersed tin oxide quantum dots, and the reaction kinetics was enhanced. The porous carbon matrix derived from Sn-BTC acts as a physical constraint to inhibit SnO<sub>2</sub> coarsening. The composite exhibits excellent cycle stability, with a capacity of 1337 mAh g<sup>-1</sup> after 200 cycles at 200 mA g<sup>-1</sup>.

The introduction of non-metallic or metallic element strategies can improve the electrochemical properties and cycle stability of tin oxide (SnO<sub>2</sub>) anode materials. Controlling the type and concentration of doped non-elements can significantly improve the conductivity of SnO<sub>2</sub>. Doping of non-metallic elements such as nitrogen (N), boron (B), etc., can introduce additional free carriers, thereby increasing the conductivity of the material.<sup>[69,70]</sup> Sulfur (S) atoms have high electronegativity and allow more free electron transport, which can change the electronic structure, crystal structure and surface chemistry of SnO<sub>2</sub>.<sup>[71]</sup> Using 2,2'-thiodiacetic acid as a source of sulfur and organic ligand, Maniyazagan *et al.* successfully designed a porous carbon SnO<sub>2</sub> doped with thioheteroatoms (Figure 5d).<sup>[72]</sup> This fully reflects the MOF's highly adjustable and structural advantages. The introduction of S improves the conductivity of the material and increases the number of lithium storage sites, providing more prominent lithium ion storage performance. The high rate capacity at 1.0 A g<sup>-1</sup> is 1188 mAh g<sup>-1</sup>. The hybridization of nano-transition metal elements such as iron (Fe), tungsten (W), etc. to achieve synergistic effects can also improve the conductivity by changing the electronic structure of SnO<sub>2</sub>.<sup>[73,74]</sup> The metal particles not only promote the decomposition of lithium oxide, but also hinder tin agglomeration and improve the mechanical integrity and electrical conductivity of the structure. He *et al.* reported for the first time that MOF-coated CoSnO<sub>3</sub> (CoSnO<sub>3</sub>@MOF) was obtained by a simple thermosolid phase reaction, and then heat-treated and transformed into SnO<sub>2</sub>/Co@C nanotubes.<sup>[38]</sup> The unique features of MOF as a sacrificial template to form interstitial-rich, uniform Co and porous carbon shells were utilized. When tested as an anode material for LIB, SnO<sub>2</sub>/Co@C nanotubes showed excellent performance. After 100 cycles, the electrode maintained a stable capacity of 800 mAh g<sup>-1</sup> at 0.2 A g<sup>-1</sup>.

Similar to tin oxide (SnO<sub>2</sub>), stannous oxide (SnO) are both potential anode materials for lithium-ion batteries, and they have some similar properties, but there are also differences. The theoretical specific capacity of SnO<sub>2</sub> is slightly higher than that of SnO. The electrochemical mechanism of SnO is as follows: SnO + 2Li<sup>+</sup> + 2e<sup>-</sup> → Sn + Li<sub>2</sub>O, Sn + xLi<sup>+</sup> + xe<sup>-</sup> ↔ Li<sub>x</sub>Sn. However, SnO generally shows better cycle stability during the lithium-ion charge and discharge cycle. In addition, SnO conductivity is generally higher than SnO<sub>2</sub>. This means that stannous oxide can conduct electrons more efficiently, thereby improving the charge transport performance of the electrode material.<sup>[22,75]</sup> However, it should be noted that the volume change of SnO during charging and discharging is still a great challenge. Bian *et al.* obtained porous SnO/carbon composites by *in situ*

pyrolysis of tin-based MOFs (Figure 5e).<sup>[22]</sup> The MOF-derived porous conductive carbon network structure has enough space to buffer the great volume change of SnO during cycling. The first discharge capacity of the SnO/C electrode was 950 mAh g<sup>-1</sup>, and even it still maintained capacity of 406 mAh g<sup>-1</sup> at 2 A g<sup>-1</sup>. In addition, Xia and co-workers reported two different tin oxides (SnO<sub>2</sub>/SnO@C) as anode materials for Li-ion batteries.<sup>[76]</sup> SnO<sub>2</sub>/SnO@C nanocomposites were obtained by the direct one-pot synthesis of Sn-PMA from 1,2,4,5-benzenetetracarboxylic acid and stannous sulfate, followed by heat treatment conversion. The SnO<sub>2</sub>/SnO@C obtained from the derivatization of MOFs showed good electrochemical stability and multiplicity properties. The capacity was still 611.9 mAh g<sup>-1</sup> after 200 cycles at 0.2 A g<sup>-1</sup>.

Tin disulfide has two kinds of lithium storage behavior, SnS<sub>2</sub> can react with lithium to transform into Li<sub>x</sub>SnS<sub>2</sub> during the cycle process, and Li<sub>x</sub>Sn alloy can also be formed to participate in it.<sup>[77,78]</sup> Specifically, SnS<sub>2</sub> + xLi<sup>+</sup> + xe<sup>-</sup> ↔ Li<sub>x</sub>SnS<sub>2</sub>, SnS<sub>2</sub> + 4Li<sup>+</sup> + 4e<sup>-</sup> → Sn + Li<sub>2</sub>S, Sn + xLi<sup>+</sup> + xe<sup>-</sup> ↔ Li<sub>x</sub>Sn. In recent years, SnS<sub>2</sub> sulfide anode materials have attracted extensive attention due to their high theoretical capacity (SnS<sub>2</sub> theoretical capacity up to 1232 mAh g<sup>-1</sup>), low cost, and large two-dimensional layer spacing.<sup>[79]</sup> Xiao and collaborators synthesized hexahedral SnS<sub>2</sub>/C microblocks from Sn-MOF precursors by vulcanization and carbonization.<sup>[80]</sup>

The layered structure of the synthesized SnS<sub>2</sub> and the porous structure of the inherited MOF reduce the volume expansion and increase the contact area between the active substance and the electrolyte. As mentioned earlier, carbon nanotube carbon networks are also used in modified SnS<sub>2</sub> anode materials in collaboration with MOF-derived carbons due to their unique one-dimensional structure and high conductivity. Xu *et al.* obtained SnS<sub>2</sub>/C/CNT materials with three-dimensional MOF carbon skeleton and one-dimensional carbon nanotube carbon network through high temperature vulcanization and solvent heat treatment (Figure 6a).<sup>[27]</sup> The SnS<sub>2</sub>/C/CNT materials under the dual-carbon modification strategy effectively retain the integrity of SnS<sub>2</sub> in the electrochemical reaction process. The porous structure increases the contact area between the material and the electrolyte and speeds up the charge transfer rate. As the electrode of lib, SnS<sub>2</sub>/C/CNT has high conductivity, high rate performance and excellent cycle stability. At the current density of 0.2 A g<sup>-1</sup>, the reversible capacity up to 954.2 mAh g<sup>-1</sup> was obtained after 100 cycles, and the capacity retention rate was 89.3%. What is more exciting is that even without the addition of conductive additives, the performance of SnS<sub>2</sub>/C/CNT materials in terms of electrochemical performance is satisfactory, which has important significance for improving the overall energy density of the battery.

Similarly, metallic stannates (MSnO<sub>4</sub>, M=Zn, Co, Mn, etc.) are also lithium-ion battery anode materials with electrochemical mechanism characteristics of transformed materials and alloy-type materials for lithium storage.<sup>[81,82]</sup> In the case of Zn<sub>2</sub>SnO<sub>4</sub>, for example, it is converted to Sn and zinc oxide/zinc nanoparticles after the first few cycles. Sn and Zn can be alloyed with lithium ions to release a strong electrochemical capacity. Yue *et al.* synthesized Zn–Sn binary MOF from Zn salt, Sn salt

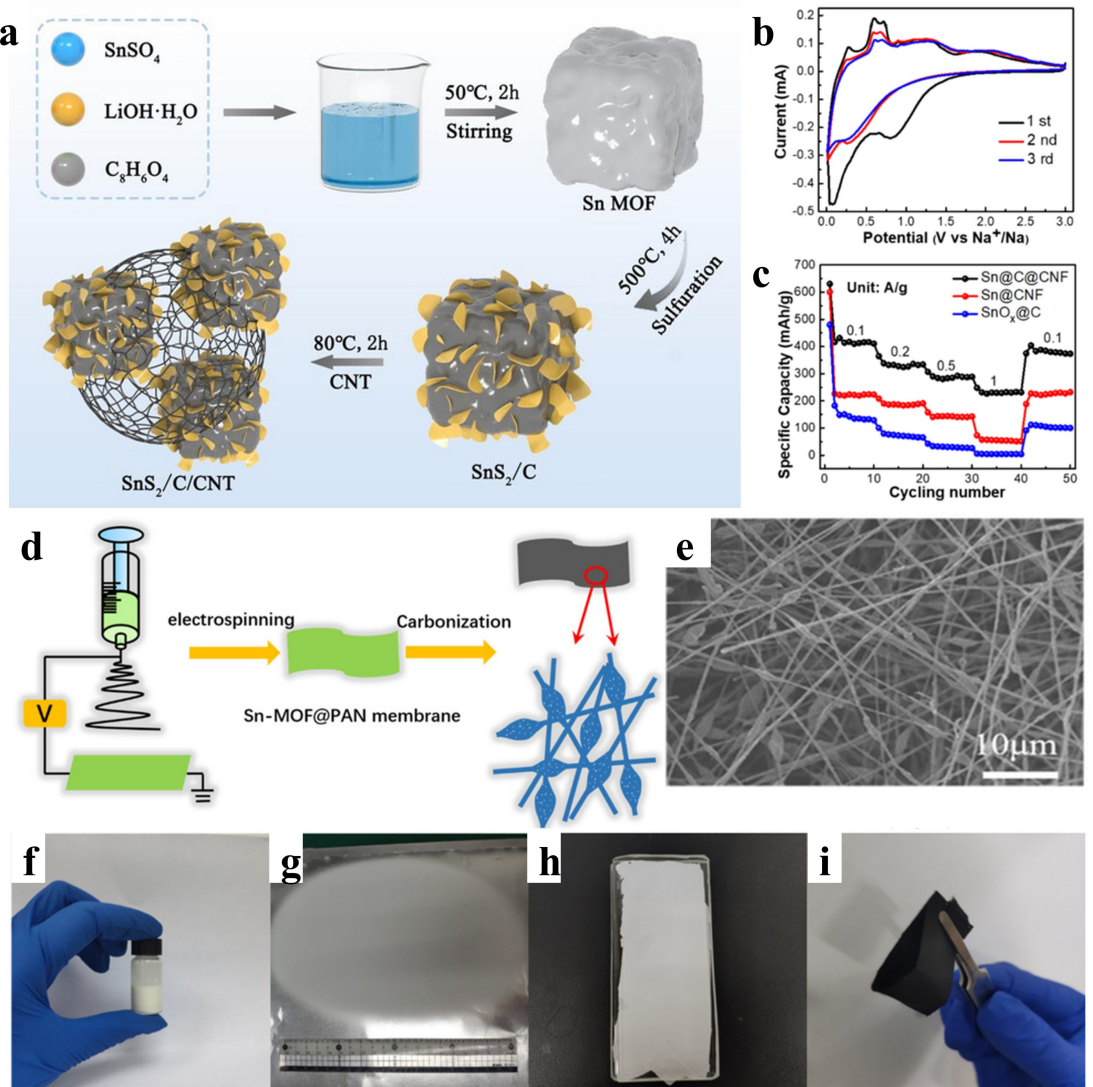


**Figure 6.** (a) Schematic illustration of the fabrication process of SnS<sub>2</sub>/C/CNT. (b) CV curve. (c) Rate performance.<sup>[27]</sup> Copyright 2023 Wiley-VCH GmbH. (d) Schematic illustration of the fabrication process of Sn-MOF@PAN-X and SCNP. (e)TEM pattern (f) solution for electrospinning, (g, h) electrospun Sn-MOF@PAN fibers on Al substrate and in quartz boat respectively, and (i) Sn-C necklace paper (SCNP).<sup>[28]</sup> Copyright 2022 Wiley-VCH GmbH.

and terephthalic acid, and obtained Zn<sub>2</sub>SnO<sub>4</sub>@C/Sn composites under H<sub>2</sub>/Ar reduction atmosphere.<sup>[83]</sup> The electrochemical measurement results show that Zn<sub>2</sub>SnO<sub>4</sub>@C/Sn anode material exhibits 1140 mAhg<sup>-1</sup> specific capacity after 100 cycles at 0.1 A g<sup>-1</sup>. This is due to the fact that nanoscale tin, as an active material and conductive agent, promotes the electron and ion transfer rate and improves the volume expansion. In addition, the storage process of lithium can be transformed from surface control to diffusion control by adjusting the calcination time to change the particle size of metal tin.

### 3.2. Sodium-ion Battery

Sodium-ion batteries are also one of the most common rechargeable batteries. Compared with lithium-ion batteries, they have some similarities in terms of working principle,

performance characteristics, and applications. Both sodium-ion and Li-ion batteries store and release electrical energy based on the migration of ions between the positive and negative electrodes and the embedding/deembedding mechanism. The difference is that the ionic radius of lithium ions is small, so the operating voltage of lithium-ion batteries is high, and the energy density is relatively high. However, the ionic radius of sodium ions is large, so the operating voltage of sodium ion batteries is low, and the energy density is relatively low.<sup>[84]</sup> Sodium is much more abundant in the Earth's crust than lithium, so sodium-ion batteries are more abundant in material resources, and relatively cheaper. Moreover, the safety performance of sodium-ion batteries is excellent, and the performance is better at high and low temperatures.<sup>[85]</sup> Therefore, sodium-ion batteries are considered to be the most promising candidate batteries for energy storage systems to replace commercial batteries such as lithium-ion batteries. The electrochemical

properties of Sn-MOF derived tin-based materials in SIBs are shown in Table 2.

### 3.2.1. Alloy Materials

Similar to lithium-ion batteries, alloy-type materials typically have a higher sodium storage capacity, which means they are able to store more sodium ions, giving them an advantage in energy storage. The application of alloy-type materials is an effective way to solve the low energy density of sodium-ion batteries and expand their practical application. Tin (Sn) is the anode material of sodium-ion battery (SIB). During charge and discharge, sodium ions will be embedded in tin lattice structure to form Na–Sn compounds, which will be removed during discharge. Therefore, tin has a high sodium storage capacity of  $847 \text{ mAh g}^{-1}$  and is considered a promising SIB electrode material.<sup>[86–87]</sup> Similarly, the design and development of reason-

ably structured Sn materials is an effective way to solve severe volume expansion and poor cycle stability and achieve specific electrochemical properties.<sup>[88]</sup>

Zhu *et al.* reported that MOF was prepared by electrospinning and added to cross-linked polyacrylonitrile (PAN) fibers. After carbothermic reduction reaction, C necklace loaded with Sn nanoparticles composite material (SCNP) was obtained, as shown in Figure 6d–6i.<sup>[28]</sup> The morphology and composition of SCNP nanofibers were optimized by changing the proportion of precursors. The conductive fiber network and large voids facilitate the transfer of electrons and ions in the electrolyte. SCNP-0.75 has good cycle stability and excellent rate performance. Run 100 cycles at  $100 \text{ mA g}^{-1}$ , maintaining the specific capacity of  $327 \text{ mAh g}^{-1}$ . At a high current density of  $2000 \text{ mA g}^{-1}$ , it has a capacity of  $207 \text{ mAh g}^{-1}$ . In addition, Zhu *et al.* had prepared interwoven CNFs thin films with layered porous structure Sn@C@CNF.<sup>[54]</sup> As shown in Figure 6b, the CV curve shows the classic characteristic peak of Sn and sodium

**Table 2.** Electrochemical properties of Sn-MOF derived tin-based materials in Other batteries.

| Materials                                                                                     | The ligand of Sn-MOF                                               | Type | Initial DC/CC(mAh g-1) | ICE (%) | CD(mA g-1)/CR/RC (mAh g-1) | Storage mechanism | Reference |
|-----------------------------------------------------------------------------------------------|--------------------------------------------------------------------|------|------------------------|---------|----------------------------|-------------------|-----------|
| SnS/NCS                                                                                       | Hexamethylene tetramine (HMTA)                                     | SIB  | 660.1/433.4            | 65.6    | 100/150/522.2              | alloy-conversion  | 23        |
| Sn/SnO@C                                                                                      | o-phthalic acid(1,2-BDC)                                           | SIB  | 1243/544               | 45      | 100/100/401                | alloy-conversion  | 25        |
| SnO@C                                                                                         |                                                                    |      | 1203/528               | 44      | 100/100/279.4              | conversion        |           |
| Sn@C                                                                                          |                                                                    |      | 1152/560               | 48      | 100/100/169.7              | alloy             |           |
| SCNP-0.75<br>( Sn–C necklace paper-0.75 g poly-acrylonitrile)                                 | terephthalic acid(1,4-BDC)                                         | SIB  | 721/442                | 58.54   | 100/100/327                | alloy             | 28        |
| SnO <sub>2</sub> /C/rGO<br>(double carbon conductive net-work-encapsulated SnO <sub>2</sub> ) | terephthalic acid(1,4-BDC)                                         | SIB  | –                      | –       | 100/150/350.7              | alloy-conversion  | 31        |
| SnS@NC@NG<br>(SnS@nitrogen-doped carbon @nitrogen-doped graphene)                             | o-phthalic acid(1,2-BDC)                                           | SIB  | 1005.2/697.8           | 69.4    | 100/100/723.3              | alloy-conversion  | 32        |
| Sn@C@CNF                                                                                      | terephthalic acid(1,4-BDC)                                         | SIB  | 690.3/485.1            | 70.5    | 100/100/360.9              | alloy             | 54        |
| SnO <sub>2</sub> /C/RGO<br>( SnO <sub>2</sub> /C/reduced graphene oxide)                      | 3,4,5-trihydroxybenzoic acid                                       | SIB  | 395.2/803.1            | 49.2    | 200/600/370.3              | alloy-conversion  | 66        |
| SnO <sub>2</sub>                                                                              | terephthalic acid(1,4-BDC)                                         | SIB  | 1030/499               | 48.4    | 50/100/430                 | alloy-conversion  | 95        |
| SnO <sub>2</sub> microporous rod                                                              | o-phthalic acid(1,2-BDC)                                           | SIB  | 1080/662               | 61.3    | 50/150/503                 | alloy-conversion  | 96        |
| SnS@C                                                                                         | 1,3,5-cyclohexanetricarboxylic acid (H <sub>3</sub> CTA)           | SIB  | 965 /861               | 89.2    | 200/100/538                | alloy-conversion  | 99        |
| N–C/SnS-500<br>(nitrogen-doped carbon/SnS composites at 500 °C)                               | 1,3,5-Triazine-2,4,6-trithiol trisodium salt (Na <sub>3</sub> tcc) | SIB  | 563.9 / 429.3          | 76.1    | 500/100/378.4              | alloy-conversion  | 101       |
| SNC2-600<br>(SnS <sub>x</sub> /C@N-Doped Carbon Nanofibers at 600 °C)                         | terephthalic acid(1,4-BDC)                                         | SIB  | 464/864                | 53.7    | 100/200/415                | alloy-conversion  | 102       |
| Sn <sub>3</sub> (PO <sub>4</sub> ) <sub>2</sub> @PC                                           | p-xylylenediphosphonic acid (H <sub>4</sub> xdp)                   | SIB  | –                      | –       | 5000/8000/202.5            | alloy-conversion  | 104       |
| Bi@Sn-C                                                                                       | 1,3,5-trimeric acid(BTC)                                           | MIB  | 659.8/328.6            | 49.8    | 100/300/324                | alloy             | 111       |

DC/CC: Discharge capacity/Charging capacity, ICE: Initial coulomb efficiency, CD: Current density, CR: Cycle number, RC: Reversible capacity.

alloying reaction,  $4\text{Sn} + 15\text{Na}^+ + 15\text{e}^- \leftrightarrow \text{Na}_{15}\text{Sn}_4$ .  $\text{Sn@C@CNF}$  still has a specific capacity of  $360.5 \text{ mAh g}^{-1}$  after 100 cycles at  $0.1 \text{ A g}^{-1}$  current density. Compared with  $\text{Sn@CNF}$  and  $\text{SnO}_x@\text{C}$ ,  $\text{Sn@C@CNF}$  has the best rate performance at 100, 200, and  $500 \text{ mA g}^{-1}$  (Figure 6c). This is because the special structure can promote  $\text{Na}^+$  storage of the active material, which is conducive to electrolyte diffusion and charge transfer. Notably, both SCNP and  $\text{Sn@C@CNF}$  act as binderless electrodes in SIBs. Binderless anode technology is a method that does not use binders in the battery manufacturing process, and this method is mainly used for the anode preparation of alkali metal batteries and other types of rechargeable batteries.<sup>[89]</sup> Due to the omission of the binder, the effective active substance content of the battery is higher, thus increasing the energy density of the battery. In addition, due to the lack of this layer of non-conductive binder, binderless anodes help to improve the conductivity and ion conductivity of the electrode. Finally, binders are eliminated in the manufacturing process, which can reduce raw material costs and processing costs, and reduce the dependence on organic solvents.<sup>[90]</sup>

### 3.2.2. Alloy-conversion Materials

Alloy-conversion materials as anode materials for sodium-ion batteries have attracted much attention in recent years.<sup>[91]</sup> These materials undergo chemical reactions during charging and discharging to achieve the storage and release of electrical energy. The working principle of the converted material is that in the charge-discharge cycle, the anode material reacts chemically with sodium ions to form Sn and  $\text{Na}_2\text{O}$ . During the charging process, Sn is transformed into a compound with a higher sodium content ( $\text{Na}_x\text{Sn}$ ); During the discharge process, these  $\text{Na}_x\text{Sn}$  dissociate and release sodium ions.<sup>[92]</sup>  $\text{SnO}_2 + 4\text{Na}^+ + 4\text{e}^- \rightarrow \text{Sn} + 2\text{Na}_2\text{O}$ ,  $\text{Sn} + x\text{Na}^+ + xe^- \leftrightarrow \text{Na}_x\text{Sn}$ . Alloy-conversion materials can usually store more sodium ions, which means they have a high theoretical capacity, which increases the energy density of the battery. In addition, their electrochemical reactions are usually accompanied by a higher voltage platform, helping to improve the voltage output stability of the battery. Tin oxide ( $\text{SnO}_2$ ) and other materials have been widely studied as anode materials for sodium-ion batteries, and have broad application prospects.<sup>[93]</sup>

However, research and improvement on the structural damage caused by the volume change of  $\text{SnO}_2$  material and the limitation of electrode reaction kinetics are also ongoing to meet future energy storage needs.<sup>[94]</sup> Lu *et al.* reported the synthesis of bimodal distribution of tin oxide nanospheres based on Sn-MOF precursors as anodes for sodium-ion batteries.<sup>[95]</sup> After 100 cycles at  $50 \text{ mA g}^{-1}$ , the  $\text{SnO}_2$  material showed a modest initial coulomb efficiency of 61.3% and a highly reversible sodium storage capacity of  $417 \text{ mAh g}^{-1}$ . When the current density is increased to  $1200 \text{ mA g}^{-1}$ , a reversible capacity of  $105 \text{ mAh g}^{-1}$  can be obtained. This is thanks to the MOF-derived increased faucet density due to the large gap of bimodal distribution of particles, thereby increasing the overall high fill sodium storage capacity of the material. The structure

and morphology of the electrode have an important effect on the electrochemical performance, which mainly involves the conductivity, surface area, porosity, ion transport rate and stability of the electrode material. In fact, the preparation path such as the concentration, ratio and temperature of the components will profoundly affect the microstructure of Sn-MOF. Therefore, Lu explored the microstructure evolution of the precursor by regulating the different concentrations of sodium hydroxide mole on the basis of the above, and thus obtained the optimal rod form of tin oxide.<sup>[96]</sup> The results show that reducing the molar concentration of sodium hydroxide can lead to an increase in Sn-MOF rod size. The porous structure and optimized rod-like structure further enhance the pseudo-capacitor charge capability and structural stability. Therefore, the electrochemical properties of tin oxide microporous rod anodes have good cyclic stability and high  $\text{Na}^+$  diffusivity. After 150 cycles, the current density is  $50 \text{ mA g}^{-1}$  and the reversible sodium storage capacity is  $503 \text{ mAh g}^{-1}$ .

Similarly, the addition of a coating of carbonaceous materials on the surface of  $\text{SnO}_2$  composites has been widely recognized and studied as an engineering in the field of sodium energy storage. Zhu and collaborators synthesized  $\text{SnO}_2/\text{C}/\text{rGO}$  composites based on MOF by adding graphene oxide (GO), an industrially mature synthesis pathway.<sup>[31]</sup> The Sn-MOF skeleton is converted into a porous carbon shell and a highly conductive reduced graphene oxide layer, and nanoscale tin oxide particles play a synergistic role to ensure that the prepared electrode has high-speed electron transfer capability and a buffer layer of active material volume expansion, showing more prominent sodium ion storage performance. After 100 cycles at  $500 \text{ mA g}^{-1}$ , the specific capacity is  $206.2 \text{ mAh g}^{-1}$ . On this basis, Yu added the green, naturally abundant product gallonic acid to the Sn-MOF/GO template to obtain the carbon-supported nano  $\text{SnO}_2$  composite of the emerging SIBs (Figure 7a).<sup>[66]</sup> The introduction of GA can interact with graphene oxide flakes and  $\text{Sn}^{2+}$  to control size, optimize surface properties, and improve dispersion. Based on electrochemical test results,  $\text{SnO}_2/\text{C}/\text{RGO}$  composites exhibit superior electrochemical properties, rapid electron and ion transport, and impressive electrochemical stability. Thus, the  $\text{SnO}_2/\text{C}/\text{RGO}$  electrode shows an impressive rate capability, and a reversible  $105.1 \text{ mAh g}^{-1}$  sodium storage capacity can be obtained at a high current density of  $5 \text{ A g}^{-1}$  (Figure 7b). After 600 cycles, the reversible specific capacity of the  $\text{SnO}_2/\text{C}/\text{RGO}$  anode remained around  $370.3 \text{ mAh g}^{-1}$  (Figure 7c).

The electrochemical dynamics of alloy-conversion materials include complex multi-step alloying processes between active substances and Na ions and some reversible conversion reactions, such as multi-component composites, sulfides, etc. Li and team used Sn-MOF as the template to prepare the hexahedral  $\text{Sn/SnO}@\text{C}$  multi-component composite material, and the hexahedral carbon frame was packed with Sn and  $\text{SnO}$  nanorods, respectively.<sup>[25]</sup> At the same time, the  $\text{SnO}@C$  and  $\text{Sn@C}$  nanocomposites were reduced by controlling different calcination temperatures. The phase information of the three composite materials is shown in Figure 7d. The experimental results show that the electrochemical performance of Sn/

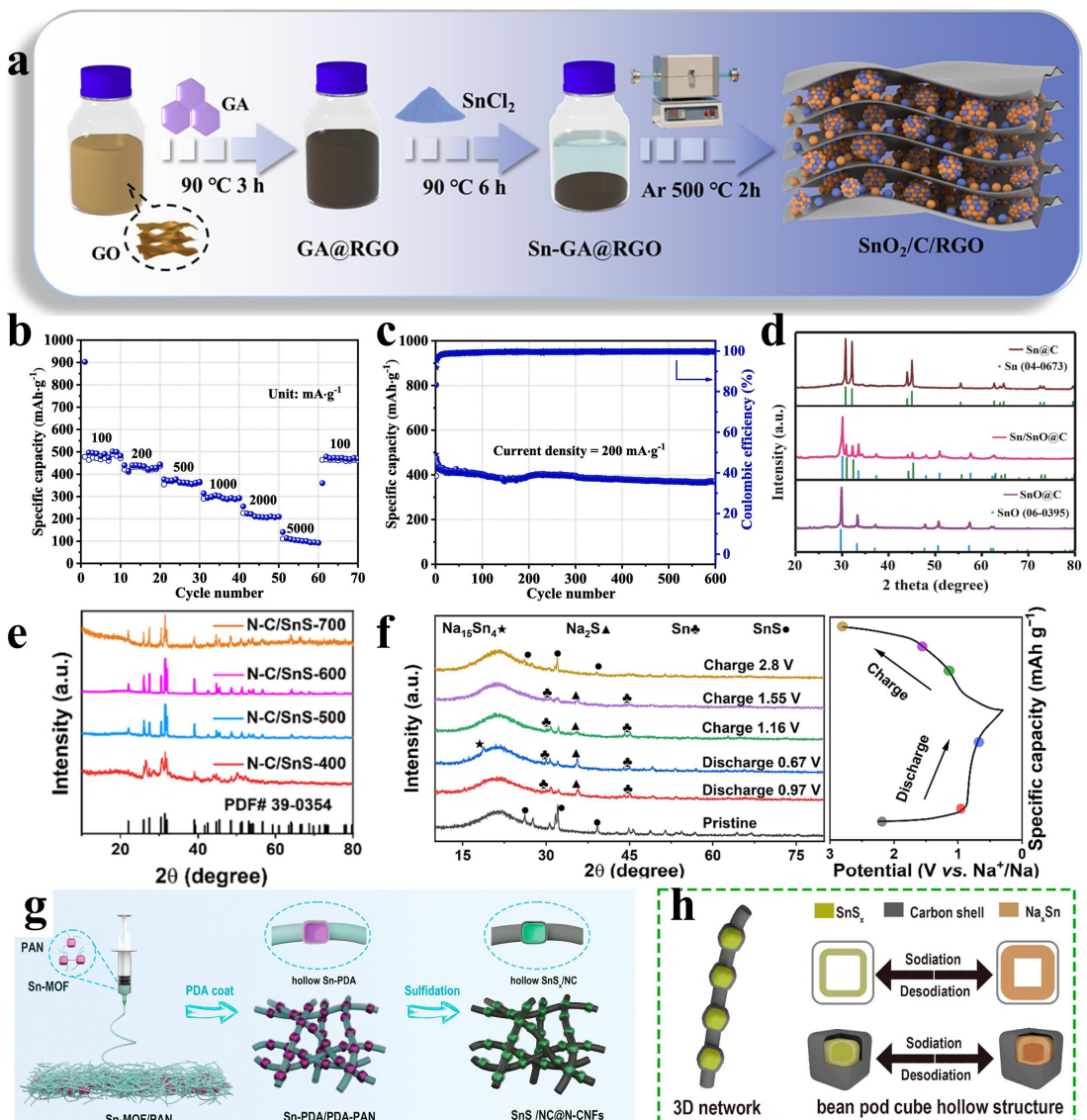


**Figure 7.** (a) Schematic illustration for the fabrication mechanism of the Sn-GA@RGO sample. (b) rate capabilities. (c) cyclic performance.<sup>[66]</sup> Copyright 2023 Elsevier Inc. (d) XRD pattern of SnO@C, Sn/SnO@C and Sn@C composites.<sup>[25]</sup> Copyright 2020 Elsevier B.V. (e) XRD pattern of the N-C/SnS series. (f) *Ex-situ* XRD patterns of N-C/SnS-500 at different voltages, corresponding to GCD curves.<sup>[101]</sup> Copyright 2023 Published by Elsevier B.V. (g) Schematic illustration of the fabrication process of MOF-SnS<sub>x</sub>/NC@N-Doped carbon nanofibers (SNC) composite. (h) scheme representation during the high-rate charge and discharge process.<sup>[102]</sup> Copyright 2024 American Chemical Society.

SnO@C is better than that of SnO@C and Sn@C. Sn/SnO@C exhibits exceptional high-speed rate performance of 516.1 mAh g<sup>-1</sup> and ultra-long cycle performance of 1401.5 mAh g<sup>-1</sup> even after 100 cycles. This is due to the unique structure derived from MOFs and the synergistic effect of different forms of active ingredients Sn/SnO.

As the anode material of sodium-ion batteries, SnS (stannous sulfide) has some unique characteristics and potential application value. SnS first undergoes the conversion reaction with sodium ions to produce Na<sub>2</sub>S, and then releases Sn to alloying with sodium ions, which has a high theoretical capacity.<sup>[97]</sup> Specifically, SnS + 2Na<sup>+</sup> + 2e<sup>-</sup> ⇌ Na<sub>2</sub>S + Sn, 4Sn + 15Na<sup>+</sup> + 2e<sup>-</sup> ⇌ Na<sub>15</sub>Sn<sub>4</sub>. In addition, because of the unique layered structure of SnS<sub>2</sub>, the interlayer distance is wide enough to allow sodium ions to pass through. Sulfur and tin are both

relatively abundant resources, so SnS as an anode material helps to reduce the cost of battery manufacturing.<sup>[98]</sup> Although SnS has many advantages, it also faces some challenges, such as capacity decay, structural changes, and so on. In Lou's work, SnS particles dispersed in a carbonaceous mesoporous framework were synthesized by a simple and convenient simultaneous carbonization and vulcanization of Sn-based MOFs as precursors (Figure 7e).<sup>[99]</sup> As a sodium storage anode, SnS@C retains a high capacity of 510 mAh g<sup>-1</sup> at the end of 200 cycles at a current density of 500 mA g<sup>-1</sup>. This is due to the advantages of unique structure and composition characteristics SnS@C composite electrode superior sodium storage performance and electronic conductivity.

In addition, the introduction of non-metallic doping in carbon materials can enhance the reactivity and conductivity of

SnS, adapt to volume changes, and provide an effective electronic conductive channel. However, the common wet chemical method for nonmetallic doping is complicated and costly, and it is difficult to ensure the uniform dispersion and controllable synthesis of each component. Using the MOFs-derived method, the composite not only inherits the structural characteristics of the MOFs precursor with porosity and high specific surface area, but also can easily obtain the nonmetallic doped carbon framework by changing the composition of the organic ligands.<sup>[100]</sup> For example, Feng *et al.* synthesized Sn-HMTA using hexamethylenetetramethylene amine (HMTA) as ligand, and then obtained nitrogen-doped carbon hybrid SnS (SnS/NCS) through annealing and vulcanization.<sup>[23]</sup> HMTA not only contains N element, but also can form highly diverse topologies with metal-ions, and two-dimensional MOFs (Sn-HMTA) can be easily synthesized. The N-doped C-layer increases the excess active site inserted by the composite Na<sup>+</sup>, which can also improve the electrical conductivity and strong mechanical support of SnS. The obtained SnS/NCS anode material has superior sodium storage properties, showing a high specific capacity of ~522 mAh g<sup>-1</sup> at 0.1 A g<sup>-1</sup> over 150 cycles, and an excellent rate capability (holding a capacity of ~321 mAh g<sup>-1</sup> at 1000 mA g<sup>-1</sup>). More interestingly, Chen *et al.* used ligand 1,3,5-Triazine-2,4,6-trithiol trisodium salt (Na<sub>3</sub>tcc) containing both S and N to synthesize N-C/SnS composites in situ through one-step carbonization and vulcan.<sup>[101]</sup> This eliminates the need to add additional S and N sources, making the synthesis step simple and efficient, saving time and economy. At the same time, they analyzed the electrochemical mechanism of the N-C/SnS-500 electrode by shifting XRD (X-ray diffraction) patterns at different voltages (Figure 7e). This can be clearly observed to correspond to the conversion reaction of SnS to Sn and sodium sulfide, while Sn undergoes the alloying reaction to produce Na<sub>15</sub>Sn<sub>4</sub> (Figure 7f). Wu et al synthesized pod cube hollow MOF-SnS<sub>x</sub>/NC@n-doped carbon nanofibers by electrospinning, PDA coating and calcination (Figure 7g).<sup>[102]</sup> Conductive nitrogen-doped carbon components can improve mechanical stability and provide electronic superhighways with enhanced surface capacitance contributions (Figure 7h). Using ideal composition and structure, SNC anodes exhibit exceptional electrochemical properties for sodium storage. In addition, the complete battery assembled with Na<sub>3</sub>V<sub>2</sub>(PO<sub>4</sub>)<sub>3</sub> as the cathode and SNC2-600 as the anode can light 34 LED bulbs, which promotes the application value of SNC composite materials in Na<sup>+</sup> batteries. Building a full battery is a necessary step in developing new battery technologies. By experimenting with different material combinations, electrolyte formulations, and battery structural designs, higher energy density, longer cycle life, and lower cost batteries are achieved. By testing the performance of the whole battery, the performance of the material in the actual battery environment can be comprehensively evaluated, including cycle stability, energy density, power density and other indicators, so as to provide an important basis for material selection and optimization. The construction of full batteries is of great significance and importance in electrochemical research, which can not only promote the progress of basic science, but also

promote the application and industrialization of battery technology.<sup>[103]</sup>

At present, as a alloy-conversion anode material, Sn<sub>3</sub>(PO<sub>4</sub>)<sub>2</sub> has a high theoretical capacity, which makes it a promising anode material in sodium-ion batteries. At the same time, Sn<sub>3</sub>(PO<sub>4</sub>)<sub>2</sub> has good chemical and thermal stability and is not prone to chemical reactions, thus ensuring the safety and cycle life of the battery.<sup>[104]</sup> It can reduce the side reaction between the electrode material and the electrolyte and reduce the self-discharge rate of the battery. Jiang and collaborators used Sn<sub>3</sub>(PO<sub>4</sub>)<sub>2</sub>@phosphorus-doped carbon (Sn<sub>3</sub>(PO<sub>4</sub>)<sub>2</sub>@PC-48) prepared by calcination of tin-based MOF precursor, and explored the working mechanism in sodium-ion batteries.<sup>[104]</sup> Alloy-conversion reaction mechanism of Sn<sub>3</sub>(PO<sub>4</sub>)<sub>2</sub>@PC-48 in sodium ion system: Sn<sub>3</sub>(PO<sub>4</sub>)<sub>2</sub> + 3Na<sup>+</sup> + 3e<sup>-</sup> ↔ Na<sub>3</sub>PO<sub>4</sub> + Sn, Sn + Na<sup>+</sup> + e<sup>-</sup> ↔ NaSn, 4NaSn + 11Na<sup>+</sup> + 11e<sup>-</sup> ↔ Na<sub>15</sub>Sn<sub>4</sub>. This work fills the gap of Sn-MOF-derived phosphate compounds as anode materials for sodium-ion batteries, and has guiding significance for the production of programmable functions and customized geometry of superstructure anode materials and the adjustment of their electrochemical properties.

### 3.3. Other Batteries

Potassium ion battery (PIBs) is a battery system belonging to alkaline ion batteries, which works similarly to lithium-ion batteries, but potassium ion batteries use potassium ion (K<sup>+</sup>) as the active ion of the battery.<sup>[105,106]</sup> Such battery systems typically include a carbon-based material or other material as an anode, and a potassium compound or potassium intercalation material as a cathode. Potassium ion batteries are considered a potential battery technology, especially in large-scale energy storage systems. Due to the relatively abundant potassium resources and low cost, potassium ion batteries can be an effective solution for applications such as power grid energy storage and smooth output of renewable energy.<sup>[107]</sup> Although potassium ion batteries show potential applications, potassium ion batteries are still in the research and development stage. The Sn<sub>3</sub>(PO<sub>4</sub>)<sub>2</sub> derived from the phosphonate MOF precursor as a self-assembled superstructure mentioned above has also been applied to potassium ion batteries (Figure 8a).<sup>[104]</sup> When evaluated as an anode material, the Sn<sub>3</sub>(PO<sub>4</sub>)<sub>2</sub> electrode showed ultra-stable cycle performance with a high reversible capacity of 202.5 mAh g<sup>-1</sup> and a capacity retention rate of 96.0% after 8,000 cycles at a current density of 5 A g<sup>-1</sup>. In addition, electrochemical kinetic analysis showed that Sn<sub>3</sub>(PO<sub>4</sub>)<sub>2</sub> also belonged to alloy-conversion anode materials, and the working mechanism was consistent with that of sodium-ion batteries (Figure 8b). First, Sn<sub>3</sub>(PO<sub>4</sub>)<sub>2</sub> crystals are converted to produce Sn and K<sub>3</sub>PO<sub>4</sub>. Then, Sn is combined with potassium ion to alloyed K<sub>4</sub>Sn<sub>23</sub> and KSn in two steps. This is the first study on the reaction mechanism of Sn<sub>3</sub>(PO<sub>4</sub>)<sub>2</sub> as the anode of PIBs. The test of the system, combined with DFT calculation (Figure 8c, 8d) and finite element analysis, showed that Sn<sub>3</sub>(PO<sub>4</sub>)<sub>2</sub>, because of its excellent hierarchical structure inherited from the MOF superstructure, ensured the compact composition of

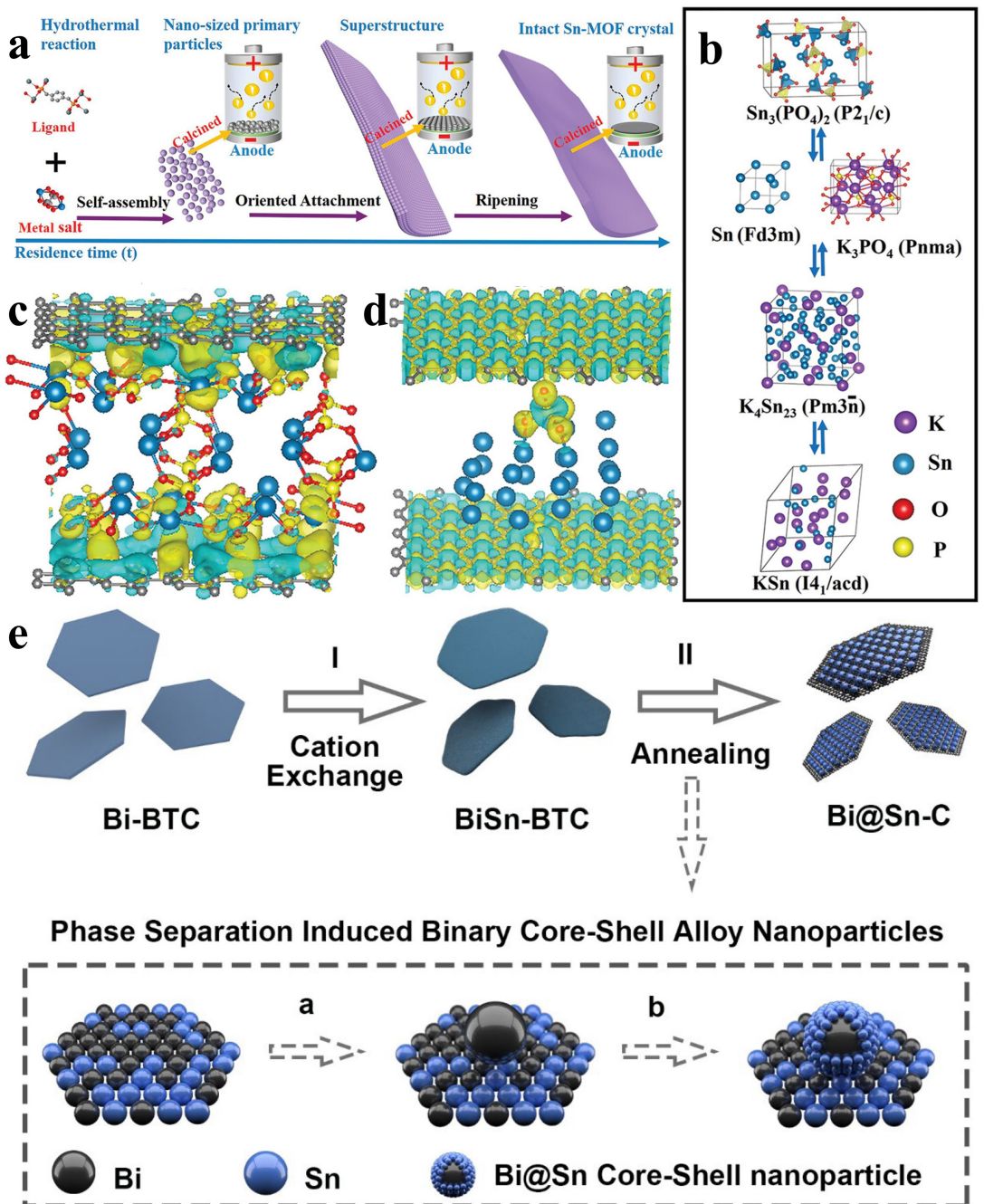


**Figure 8.** (a) Schematic illustration for the fabrication mechanism of the Sn-MOF precursors and the applications as anode materials in batteries. (b) The schematic illustration of the reaction mechanism for  $\text{Sn}_3(\text{PO}_4)_2 @ \text{PC}$ . (c) Charge-density difference of  $\text{Sn}_3(\text{PO}_4)_2 @ \text{PC}$ . (d) Charge-density difference of caused by  $\text{PO}_4^{3-}$  in Sn@PC. Copyright 2023 The Authors.<sup>[104]</sup> Advanced Science published by Wiley-VCH GmbH. (e) Schematic illustration for the fabrication mechanism of Bi@Sn alloy nanoparticles embedded in carbon sheets.<sup>[111]</sup> Copyright 2022 American Chemical Society

interconnected nanoparticles and the stability of the overall structure. This enhances the  $\text{K}^+$  ion storage dynamics and reduces the impediments to electron transport, controlling the material's huge volume expansion.

A magnesium ion battery is a battery system that uses magnesium ion ( $\text{Mg}^{2+}$ ) as the active ion of the battery. Compared with traditional lithium-ion batteries, magnesium ion batteries have potential advantages, such as abundant magnesium resources, low cost, relatively high electrochemical

stability, etc..<sup>[108]</sup> In addition, the sedimentary layer of electro-deposited Mg metal is smooth and uniform, which reduces the possibility of metal dendrite growth and ensures the safety of the battery to a greater extent.<sup>[109]</sup> Magnesium ion battery is considered as a potential battery technology and is becoming one of the research hotspots in the field of materials science and battery technology. The alloy type Sn anode material has a higher theoretical capacity ( $903 \text{ mAh g}^{-1}$ ) and a lower operating voltage in magnesium ion batteries.<sup>[110]</sup> However, in addition to

the volume expansion, the high diffusion barrier of  $Mg^{2+}$  in Sn may limit the charge and discharge rate of the battery and affect the power performance of the battery. Chen *et al.* prepared the bimetallic frame BiSn-BTC by hydrothermal method and ion exchange method and embedded it in two-dimensional carbon sheet binary Bi@Sn alloy nanoparticles (Bi@Sn-C), as shown in Figure 8e.<sup>[11]</sup> Interestingly, the binary core-shell Bi@Sn alloy nanoparticles were obtained by phase separation during heat treatment using the difference between the melting points of Bi and Sn. It is clever that the bielemental active metals Bi and Sn with different alloy potentials are conducive to improving the structural stability and magnesium storage kinetics of alloy-based anodes. The alternating alloy reactions at different potentials form a guarantee of mutual restraint. In addition, the derived porous carbon framework and nano-metal site design improve the electrical conductivity, enrich the active site, and enhance the Mg binding ability. As a magnesium ion battery anode material, the Bi@Sn-C electrode provides an ideal 200  $mAh g^{-1}$  at a high rate of 500  $mA g^{-1}$ . After 100 cycles, the reversible specific capacity at 100  $mA g^{-1}$  is 214  $mAh g^{-1}$ . These studies provide design strategies and implications for the development of advanced MIBs multi-element alloy materials using MOF precursors.

#### 4. Conclusion and Prospect

Overall, the development of metal-ion batteries has far-reaching implications for promoting clean energy, improving energy storage efficiency, and facilitating the sustainable development of electric vehicles and renewable energy. Different types of metal-ion batteries are required to overcome different challenges, which have led to research and advances in battery materials, structures, and fabrication technologies. This paper reviews the use of Sn-MOFs as sacrificial template-derived tin-based materials as anode materials for advanced batteries such as lithium-ion batteries, sodium-ion batteries, potassium-ion batteries and magnesium-ion batteries. The tin-based materials obtained by using MOF derivation possess unique advantages: I. Inheriting the inherent properties of the precursor's large surface area and highly ordered structure with pore size distribution. II. Easily introduce abundant nanoscale metallic (Fe, Ni, Cu, etc.) and non-metallic elements (C, N, S, etc.). III. The chemically derived components are well dispersed and fully coordinated. IV. Design and construction of new derivatives by precisely adjusting the chemical composition and reaction conditions of the desired MOF precursors.

For metal-ion batteries with Sn-based anodes, the most important challenges common to both energy storage mechanism materials today are the volumetric changes and structural destabilization of the electrode materials. In recent years, the use of highly conductive carbon materials (e.g., graphene, carbon nanotubes, porous carbon, carbon fibers) as a robust and conductive matrix for Sn-based materials has been the main optimization strategy. In addition, the introduction of non-metals/metals to design a rational alloying or doping strategy is key. The introduction of multielemental materials

can make Sn-based materials combine multifunctional properties such as increased electrical conductivity, improved catalytic activity, and enhanced structural stability. Theoretically and experimentally designing and precisely controlling ideal fine structures and compositions, such as surface modification, coating or flexible treatment, can enhance the stability of the materials and inhibit the expansion or dissolution of the structure, thus improving the cycle life and cycle stability of the materials.

In addition to the above mentioned strategies, further development of tin-based anodes for rechargeable batteries and future research directions include the following aspects: I. To explore improved synthesis methods of tin-based anode materials to achieve higher crystallinity, more uniform particle distribution and better electrochemical performance. The use of new template agent, interface regulator and other methods or the development of advanced electrode preparation technology (such as spraying method, sol-gel method, electrochemical deposition method, etc.) to achieve the uniform distribution and efficient utilization of tin-based anode materials in large areas and high-density electrodes, optimize the structure and performance of tin-based materials. II. Alloying or compounding tin with other metals or carbon materials to improve the stability and capacity of tin-based anodes. Explore new combinations of alloyed and compounded materials to achieve higher specific capacity and longer cycle life. III. Research and optimize the electrolyte formula and electrode interface engineering of lithium-ion batteries to reduce solid-liquid interface resistance, inhibit the formation of solid electrolyte interface layer, and improve the cycle stability and rate performance of batteries. IV. Using advanced characterization techniques and computational simulation methods, the structure, phase transition behavior and electrochemical mechanism of tin-based anode materials were deeply studied to provide theoretical guidance and scientific basis for material design and performance optimization.

Although Sn-MOF-derived tin-based materials have many potential advantages in metal-ion batteries, further improvement and development are needed. First of all, the performance of anode materials developed in the laboratory may perform well on a small scale, but in large-scale applications, its performance may be affected by batch differences in material preparation, different production conditions and other factors, resulting in unstable performance. Secondly, the raw material cost, production cost and yield of MOF hinder its large-scale application. Finally, in the research of anode materials, consider replacing toxic or non-renewable elements in traditional materials, using more environmentally friendly materials, advocating efficient and sustainable synthesis methods, in line with the principles of green chemistry. In conclusion, the study of anodic materials for Sn-MOF derived tin-based materials has promoted the development of materials science and provided an important foundation for in-depth understanding of electrochemical processes, energy storage mechanisms and material properties. Advances in these areas will lead to innovation and sustainability in the field of energy storage and conversion in the future.

## Acknowledgements

We gratefully acknowledge the financial support from the Research and Development Plan Project in Key Fields of Guangdong Province (2020B0101030005). Furthermore, the authors would like to thank Shiyanjia Lab ([www.shiyanjia.com](http://www.shiyanjia.com)).

## Conflict of Interests

There is no conflict of interest to report.

## Data Availability Statement

Data will be made available on request.

**Keywords:** Sn-based anode · MOFs · alloy materials · alloy-conversion materials

- [1] Z. Bai, Q. Yao, M. Wang, W. Meng, S. Dou, H.-k. Liu, N. Wang, *Adv. Energy Mater.* **2024**, 2303788.
- [2] Z. Huang, Z. Gu, Y. Heng, E. H. Ang, H. Geng, X. Wu, *Chem. Eng. J.* **2023**, 452, 139438.
- [3] A. K. Prajapati, A. Bhatnagar, *J. Energy Chem.* **2023**, 83, 509.
- [4] H. Zhao, J. Li, Q. Zhao, X. Huang, S. Jia, J. Ma, Y. Ren, *Electrochem. Energy Rev.* **2024**, 7, 11.
- [5] S. Chae, M. Ko, K. Kim, K. Ahn, J. Cho, *Joule* **2017**, 1, 47.
- [6] F. Wu, J. Maier, Y. Yu, *Chem. Soc. Rev.* **2020**, 49, 1569.
- [7] R. Liu, N. Li, E. Zhao, J. Zhao, L. Yang, W. Wang, H. Liu, C. Zeng, *Mater. Futures* **2022**, 1, 045102.
- [8] R. Schmuck, R. Wagner, G. Hörpel, T. Placke, M. Winter, *Nat. Energy* **2018**, 3, 267.
- [9] D. Chao, C. Zhu, P. Yang, X. Xia, J. Liu, J. Wang, X. Fan, S. V. Savilov, J. Lin, H. J. Fan, *Nat. Commun.* **2016**, 7, 12122.
- [10] Y. Yang, X. Liu, Z. Dai, F. Yuan, Y. Bando, D. Golberg, X. Wang, *Adv. Mater.* **2017**, 29, 1606922.
- [11] W. Zhang, Y. Liu, Z. Guo, *Sci. Adv.* **2019**, 5, 7412.
- [12] A. Indra, T. Song, U. Paik, *Adv. Mater.* **2018**, 30, 1705146.
- [13] P. W. Menezes, A. Indra, V. Gutkin, M. Driess, *Chem. Commun.* **2017**, 53, 8018.
- [14] X. Wu, M. Liu, H. Guo, S. Ying, Z. Chen, *Chin. J. Struct. Chem.* **2021**, 40, 994.
- [15] Y. Zhao, Z. Song, X. Li, Q. Sun, N. Cheng, S. Lawes, X. Sun, *Energy Storage Mater.* **2016**, 2, 35.
- [16] N. Wu, W. Wang, L. Q. Kou, X. Zhang, Y. R. Shi, T. H. Li, F. Li, J. M. Zhou, Y. Wei, *Chem. Eur. J.* **2018**, 24, 6330.
- [17] Y. Wu, N. Xie, X. Li, Z. Fu, X. Wu, Q. Zhu, *Chin. J. Struct. Chem.* **2021**, 40, 1346.
- [18] G. M. Tomboc, Y. Wang, H. Wang, J. Li, K. Lee, *Energy Storage Mater.* **2021**, 39, 21.
- [19] Y. Liu, Y. Li, H. Kang, T. Jin, L. Jiao, *Mater. Horiz.* **2016**, 3, 402.
- [20] J. Qin, C. He, N. Zhao, Z. Wang, C. Shi, E.-Z. Liu, J. Li, *ACS Nano* **2014**, 8, 1728.
- [21] Z. Zhu, S. Wang, J. Du, Q. Jin, T. Zhang, F. Cheng, J. Chen, *Nano Lett.* **2014**, 14, 153.
- [22] Z. Bian, A. Li, R. He, H. Song, X. Chen, J. Zhou, Z. Ma, *Electrochim. Acta* **2018**, 289, 389.
- [23] S. Feng, L. Ma, J. Lin, X. Lu, L. Xu, J. Wu, X. Yan, X. Fan, *Electrochim. Acta* **2021**, 387, 138535.
- [24] J. Hong, Y. Liu, L. Liu, H. Liang, X. Huang, *J. Alloys Compd.* **2024**, 970, 172374.
- [25] X. Li, C. He, J. Zheng, W. Ye, W. Yin, B. Tang, Y. Rui, *J. Alloys Compd.* **2020**, 842, 155605.
- [26] K. Xu, L. Ma, X. Shen, Z. Ji, A. Yuan, L. Kong, G. Zhu, J. Zhu, *Electrochim. Acta* **2019**, 323, 134855.
- [27] Z. Xu, W. Lv, T. Zhang, Z. Ye, Q. Li, D. Jin, H. Qiu, *Energy Technol.* **2024**, 12, 2300890.
- [28] Z. Xu, J. Ye, Y. Pan, K. Liu, X. Liu, J. Shui, *Energy Technol.* **2022**, 10, 2101024.
- [29] Q. Zhao, D. Zhao, L. Feng, J. Yu, Y. Liu, S. Guo, *J. Mater.* **2023**, 9, 362.
- [30] X. Zhou, S. Chen, J. Yang, T. Bai, Y. Ren, H. Tian, *ACS Appl. Mater. Interfaces* **2017**, 9, 14309.
- [31] S. Zhu, A. Huang, Q. Wang, Y. Xu, *Nanotechnology* **2021**, 32, 305403.
- [32] Q. Cheng, X. Yu, *J. Mater. Chem. A* **2021**, 9, 11381.
- [33] H. Fu, C. Shi, J. Nie, J. Xie, S. Yao, *J. Solid State Electrochem.* **2022**, 26, 2919.
- [34] R. Dai, W. Sun, L. P. Lv, M. Wu, H. Liu, G. Wang, Y. Wang, *Small* **2017**, 13, 1700521.
- [35] M. Cognet, J. Condomines, J. Cambedouzou, S. Madhavi, M. Carboni, D. Meyer, *J. Hazard. Mater.* **2020**, 385, 121603.
- [36] M. Kim, M. Kim, J. Park, J. Kim, C. Ahn, A. Jin, J. Mun, Y. Sung, *Nanoscale* **2020**, 12, 15214.
- [37] N. Brainer, T. dos Santos, C. D. Barbosa, S. Meneghetti, *Mater. Lett.* **2020**, 280, 128512.
- [38] Q. He, J. Liu, Z. Li, Q. Li, L. Xu, B. Zhang, J. Meng, Y. Wu, L. Mai, *Small* **2017**, 13, 1701504.
- [39] Q. Jiang, J. Li, Y. Yang, Y. Ren, L. Dai, J. Gao, L. Wang, J. Ye, Z. He, *Rare Met.* **2023**, 42, 1214.
- [40] J. Liu, D. Xie, X. Xu, L. Jiang, R. Si, W. Shi, P. Cheng, *Nat. Commun.* **2021**, 12, 3131.
- [41] R. Shah, S. Ali, F. Raziq, S. Ali, P. M. Ismail, S. Shah, R. Iqbal, X. Wu, W. He, X. Zu, *Coord. Chem. Rev.* **2023**, 477, 214968.
- [42] L. Sun, H. Wang, S. Zhai, J. Sun, X. Fang, H. Yang, D. Zhai, C. Liu, W. Deng, H. Wu, *J. Energy Chem.* **2023**, 76, 368.
- [43] J. Ren, Y. Huang, H. Zhu, B. Zhang, H. Zhu, S. Shen, G. Tan, F. Wu, H. He, S. Lan, *Carbon Energy* **2020**, 2, 176.
- [44] J. Lin, R. C. K. Reddy, C. Zeng, X. Lin, A. Zeb, C.-Y. Su, *Coord. Chem. Rev.* **2021**, 446, 214118.
- [45] K. Liu, C. Li, L. Yan, M. Fan, Y. Wu, X. Meng, T. Ma, *J. Mater. Chem. A* **2021**, 9, 27234.
- [46] G. A. Elia, S. Panero, A. Savoini, B. Scrosati, J. Hassoun, *Electrochim. Acta* **2013**, 90, 690.
- [47] X. Fan, P. Dou, A. Jiang, D. Ma, X. Xu, *ACS Appl. Mater. Interfaces* **2014**, 6, 22282.
- [48] L. Ben, J. Zhou, H. Ji, H. Yu, W. Zhao, X. Huang, *Mater. Futures* **2022**, 1, 015101.
- [49] X. Li, A. Dhanabalan, L. Gu, C. Wang, *Adv. Energy Mater.* **2012**, 2, 238.
- [50] H. Liu, S. Wang, J. Zhao, B. Zhang, L. Liu, R. Bao, Z. Jing, *J. Energy Storage* **2024**, 80, 109862.
- [51] Y. Hu, Y. Yin, M. Zhang, Z. Wu, Z. Shen, *Chin. J. Struct. Chem.* **2021**, 40, 1513.
- [52] J. Asenbauer, D. Horny, M. Olutogun, K. Schulz, D. Bresser, *Mater. Futures* **2024**, 3, 015101.
- [53] F. Pan, Y. Cao, M. Xu, L. Shao, J. Sun, A. Chen, *Mater. Lett.* **2020**, 273, 127909.
- [54] S. Zhu, A. Huang, Q. Wang, Y. Xu, *Nanotechnology* **2021**, 32, 165401.
- [55] R. Dai, W. Sun, Y. Wang, *Electrochim. Acta* **2016**, 217, 123.
- [56] R. Kim, D. Choi, K.-Y. Shin, D. Han, *J. Alloys Compd.* **2021**, 879, 160416.
- [57] J. Li, X. Xu, Z. Luo, C. Zhang, Y. Zuo, T. Zhang, P. Tang, M. F. Infante-Carrío, J. Arbiol, J. Llorca, *ChemSusChem* **2019**, 12, 1451.
- [58] Y. Liu, L. Wang, K. Jiang, S. Yang, *J. Alloys Compd.* **2019**, 775, 818.
- [59] H. Shi, Z. Fang, X. Zhang, F. Li, Y. Tang, Y. Zhou, P. Wu, G. Yu, *Nano Lett.* **2018**, 18, 3193.
- [60] H. Wang, X. Du, X. Jiang, Y. Chai, X. Yang, R. Yuan, *Chem. Eng. J.* **2017**, 313, 535.
- [61] R. Gao, J. Tang, S. Tang, K. Zhang, K. Ozawa, L.-C. Qin, *Electrochim. Acta* **2022**, 410, 140036.
- [62] Y. Kim, H. Hwang, C. S. Yoon, M. G. Kim, J. Cho, *Adv. Mater.* **2007**, 19, 92.
- [63] Z. Liu, J. Chen, X. Fan, Y. Pan, Y. Li, L. Ma, H. Zhai, L. Xu, *J. Alloys Compd.* **2021**, 871, 159531.
- [64] X. Zhou, Z. Geng, C. Zhang, J. Wang, D. Wang, *J. Energy Chem.* **2015**, 24, 529.
- [65] X. Lu, Y. Chen, Q. Tian, W. Zhang, Z. Sui, J. Chen, *Appl. Surf. Sci.* **2021**, 537, 148052.
- [66] L. Yu, R. Zhang, R. Jia, W. Fa, H. Yin, L. Y. Zhang, H. Li, B. Xu, *J. Colloid Interface Sci.* **2024**, 653, 359.
- [67] C. Liang, J. Guo, L. Yue, M. Wang, J. Liang, X. Wang, Y. Li, K. Yu, *Diamond Relat. Mater.* **2023**, 140, 110488.
- [68] K. Gong, Y. Ma, T. Zhang, L. Yan, Y. Miao, F. Gao, *Adv. Eng. Mater.* **2021**, 23, 2100064.

- [69] L. Li, J. Zhang, Y. Zou, W. Jiang, W. Lei, Z. Ma, *J. Electroanal. Chem.* **2019**, 833, 573.
- [70] X. Wang, X. Cao, L. Bourgeois, H. Guan, S. Chen, Y. Zhong, D. M. Tang, H. Li, T. Zhai, L. Li, *Adv. Funct. Mater.* **2012**, 22, 2682.
- [71] J. Ou, L. Yang, Z. Zhang, X. Xi, *J. Power Sources* **2016**, 333, 193.
- [72] M. Maniyazagan, P. Naveenkumar, H. Zuhair, H.-W. Yang, W. S. Kang, S.-J. Kim, *Solid State Sci.* **2023**, 136, 107091.
- [73] Y. Feng, K. Wu, J. Ke, X. Huang, C. Bai, H. Dong, D. Xiong, M. He, *Appl. Surf. Sci.* **2020**, 533, 147508.
- [74] F. Mueller, D. Bresser, V. S. K. Chakravadhanula, S. Passerini, *J. Power Sources* **2015**, 299, 398.
- [75] Y. Cheng, J. Huang, J. Li, L. Cao, H. Qi, *Nano Lett.* **2018**, 13, 257.
- [76] S. Xia, Y. Yan, W. Huang, R. Yang, H. Suo, J. Liu, F. Cheng, J. Liu, *J. Power Sources* **2020**, 464, 228247.
- [77] C. Cao, H. Dong, F. Liang, Y. Zhang, W. Zhang, H. Wang, H. Shao, H. Liu, K. Dong, Y. Tang, *Chem. Eng. J.* **2021**, 416, 129094.
- [78] J. Wang, H. Wang, T. Yao, T. Liu, Y. Tian, C. Li, F. Li, L. Meng, Y. Cheng, *J. Colloid Interface Sci.* **2020**, 560, 546.
- [79] R. Li, C. Miao, L. Yu, H. Mou, M. Zhang, W. Xiao, *Solid State Ionics* **2020**, 348, 115288.
- [80] X. Xiao, F. Zhao, J. Liu, Z. Wang, Q. Sui, M. Tan, *Mater. Lett.* **2021**, 296, 129877.
- [81] L. Cui, X. Li, C. Yin, J. Wang, S. Li, Q. Zhang, S. Kang, *Dalton Trans.* **2019**, 48, 504.
- [82] G. Wang, Z. Liu, P. Liu, *Electrochim. Acta* **2011**, 56, 9515.
- [83] H. Yue, Z. Shi, L. Wang, X. Li, H. Dong, Y. Yin, S. Yang, *J. Alloys Compd.* **2017**, 723, 1018.
- [84] K. Wang, H. Zhuo, J. Wang, F. Poon, X. Sun, B. Xiao, *Adv. Funct. Mater.* **2023**, 33, 2212607.
- [85] J. Peng, W. Zhang, Q. Liu, J. Wang, S. Chou, H. Liu, S. Dou, *Adv. Mater.* **2022**, 34, 2108384.
- [86] M. Lao, Y. Zhang, W. Luo, Q. Yan, W. Sun, S. X. Dou, *Adv. Mater.* **2017**, 29, 1700622.
- [87] X. Xie, K. Kretschmer, J. Zhang, B. Sun, D. Su, G. Wang, *Nano Energy* **2015**, 13, 208.
- [88] M. Tan, S. Han, Z. Li, H. Cui, D. Lei, C. Wang, *Nano Res.* **2023**, 16, 3804.
- [89] D. J. Kirsch, S. D. Lacey, Y. Kuang, G. Pastel, H. Xie, J. W. Connell, Y. Lin, L. Hu, *ACS Appl. Energ. Mater.* **2019**, 2, 2990.
- [90] T. M. Huggins, J. M. Whiteley, C. T. Love, K. Lee, S.-H. Lee, Z. J. Ren, J. C. Biffinger, *ACS Appl. Mater. Interfaces* **2016**, 8, 26868.
- [91] H. Xu, H. Li, X. Wang, *ChemElectroChem* **2023**, 10, e202201151.
- [92] H. Kim, D. I. Kim, W.-S. Yoon, *J. Electrochem. Sci. Technol.* **2022**, 13, 32.
- [93] S. Oro, K. Urita, I. Moriguchi, *Chem. Lett.* **2017**, 46, 502.
- [94] H. Li, X. Jia, B. Huang, J. Yang, Y. Li, S. Zhong, *Nanotechnology* **2023**, 34, 325602.
- [95] X. Lu, F. Luo, Q. Xiong, H. Chi, H. Qin, Z. Ji, L. Tong, H. Pan, *Mater. Res. Bull.* **2018**, 99, 45.
- [96] X. Lu, Q. Xiong, Z. Yao, J. Qiu, Y. Xu, R. Shan, X. He, Y. Cai, *Nanotechnology* **2021**, 32, 485403.
- [97] J. Mei, J. Han, F. Wu, Q. Pan, F. Zheng, J. Jiang, Y. Huang, H. Wang, K. Liu, Q. Li, *Front. Chem.* **2023**, 10, 1105997.
- [98] J. Zhu, D. Wang, T. Liu, *Ionics* **2014**, 20, 141.
- [99] X. Luo, J. Shao, P. He, K. Li, W. Zhao, *J. Solid State Chem.* **2022**, 307, 122736.
- [100] Y. Chen, M. Lu, J.-E. Zhou, X. Zhang, Y. Li, X. Lin, A. Zeb, Z. Xu, *Electrochim. Acta* **2022**, 435, 141355.
- [101] F. Chen, W. Shuang, Y. Wang, L. Yang, Z. Bai, *Appl. Surf. Sci.* **2024**, 645, 158686.
- [102] C. Wu, Z. Long, H. Dai, Z. Li, H. Qiao, K. Liu, Q. Wang, K. Wang, Q. Wei, *ACS Appl. Mater. Interfaces* **2024**, 16 (8), 10545.
- [103] N. LeGe, X. He, Y. Wang, Y. Lei, Y. Yang, J. Xu, M. Liu, X. Wu, W. Lai, S. Chou, *Energy Environ. Sci.* **2023**, 16, 5688.
- [104] H. Jiang, S. Zhang, L. Yan, Y. Xing, Z. Zhang, Q. Zheng, J. Shen, X. Zhao, L. Wang, *Adv. Sci.* **2023**, 10, 2206587.
- [105] J. Y. Hwang, S. T. Myung, Y. K. Sun, *Adv. Funct. Mater.* **2018**, 28, 1802938.
- [106] J. Li, W. Zhang, W. Zheng, *Small* **2024**, 20, 2305021.
- [107] J. C. Pramudita, D. Sehrawat, D. Goonetilleke, N. Sharma, *Adv. Energy Mater.* **2017**, 7, 1602911.
- [108] R. Shah, V. Mittal, E. Matsil, A. Rosenkranz, *Adv. Mech. Eng.* **2021**, 13(3), 1–9.
- [109] J. Niu, Z. Zhang, D. Aurbach, *Adv. Energy Mater.* **2020**, 10, 2000697.
- [110] N. Singh, T. S. Arthur, C. Ling, M. Matsui, F. Mizuno, *Chem. Commun.* **2013**, 49, 149.
- [111] C. Chen, H. Huang, R. Hu, R. Bi, L. Zhang, *ACS Appl. Mater. Interfaces* **2022**, 14, 39965.

Manuscript received: April 4, 2024

Revised manuscript received: May 19, 2024

Accepted manuscript online: May 31, 2024

Version of record online: July 22, 2024